

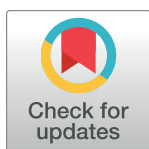
## RESEARCH ARTICLE

# Design, synthesis, anti-proliferative evaluation, docking, and MD simulations studies of new thiazolidine-2,4-diones targeting VEGFR-2 and apoptosis pathway

Mohammed S. Taghour<sup>1</sup>, Hazem Elkady<sup>1</sup>, Wagdy M. Eldehna<sup>2</sup>, Nehal El-Deeb<sup>3,4</sup>, Ahmed M. Kenawy<sup>5</sup>, Eslam B. Elkaeed<sup>6</sup>, Bshra A. Alsouk<sup>7</sup>, Mohamed S. Alesawy<sup>1</sup>, Dalal Z. Husein<sup>8</sup>, Ahmed M. Metwaly<sup>4,9\*</sup>, Ibrahim H. Eissa<sup>1\*</sup>

**1** Pharmaceutical Medicinal Chemistry & Drug Design Department, Faculty of Pharmacy (Boys), Al-Azhar University, Cairo, Egypt, **2** Department of Pharmaceutical Chemistry, Faculty of Pharmacy, Kafrelsheikh University, Kafrelsheikh, Egypt, **3** Biopharmaceutical Products Research Department, Genetic Engineering and Biotechnology Research Institute, City of Scientific Research and Technological Applications (SRTA-City), Alexandria, Egypt, **4** Pharmaceutical and Fermentation Industries Development Center, City of Scientific Research and Technological Applications (SRTA City), Alexandria, Egypt, **5** Nucleic Acids Research Department, Genetic Engineering and Biotechnology Research Institute, City of Scientific Research and Technological Applications (SRTA-City), Alexandria, Egypt, **6** Department of Pharmaceutical Sciences, College of Pharmacy, AlMaarefa University, Riyadh, Saudi Arabia, **7** Department of Pharmaceutical Sciences, College of Pharmacy, Princess Nourah Bint Abdulrahman University, Riyadh, Saudi Arabia, **8** Chemistry Department, Faculty of Science, New Valley University, El-Kharja, Egypt, **9** Pharmacognosy and Medicinal Plants Department, Faculty of Pharmacy (Boys), Al-Azhar University, Cairo, Egypt

\* [Ibrahimeissa@azhar.edu.eg](mailto:Ibrahimeissa@azhar.edu.eg) (IHE); [ametwaly@azhar.edu.eg](mailto:ametwaly@azhar.edu.eg) (AMM)



## OPEN ACCESS

**Citation:** Taghour MS, Elkady H, Eldehna WM, El-Deeb N, Kenawy AM, Elkaeed EB, et al. (2022) Design, synthesis, anti-proliferative evaluation, docking, and MD simulations studies of new thiazolidine-2,4-diones targeting VEGFR-2 and apoptosis pathway. PLoS ONE 17(9): e0272362. <https://doi.org/10.1371/journal.pone.0272362>

**Editor:** Mohammad Shahid, Aligarh Muslim University, INDIA

**Received:** May 4, 2022

**Accepted:** July 18, 2022

**Published:** September 23, 2022

**Copyright:** © 2022 Taghour et al. This is an open access article distributed under the terms of the [Creative Commons Attribution License](https://creativecommons.org/licenses/by/4.0/), which permits unrestricted use, distribution, and reproduction in any medium, provided the original author and source are credited.

**Data Availability Statement:** All relevant data are within the paper and its [Supporting Information](#) files.

**Funding:** This research was funded by Princess Nourah bint Abdulrahman University Researchers Supporting Project number (PNURSP2022R142), Princess Nourah bint Abdulrahman University, Riyadh, Saudi Arabia. The authors extend their appreciation to the Research Center at AlMaarefa University for funding this work. The funders had

## Abstract

We report herein, the design and synthesis of thiazolidine-2,4-diones derivatives as new inhibitors for VEGFR-2. The designed members were assessed for their *in vitro* anticancer activity against four cancer cell lines; A549, Caco-2, HepG-2 and MDA-MB-231. Compound **14a** showed the most potent effects against Caco-2, and HepG-2 cell lines (IC<sub>50</sub> = of 1.5 and 31.5 μM, respectively). Next, the *in vitro* VEGFR-2 inhibitory activity, safety profiles and selectivity indices were examined for all the synthesized members against the normal Vero cell line. Compound **14a** (the safest member against Caco-2 cell line) was further investigated for its ability to inhibit Caco-2 cells migration and healing. Moreover, the apoptotic induction of compound **14a** against Caco-2 cell line was investigated by assessing against four apoptotic genes (Bcl2, Bcl-xl, TGF, and Survivin). The results revealed that compound **14a** can exert apoptosis through significant reduction of Bcl2, Survivin, and TGF gene expression levels. Finally, deep computational studies including molecular docking, ADMET, toxicity studies, and MD simulation were carried out. Also, the DFT calculations were performed and discussed, and the results confirmed the inhibitory reactivity of **14a** against VEGFR-2. Compound **14a** is expected to be used as a potential lead in the development of new VEGFR-2 inhibitors with increased potency.

no role in study design, data collection and analysis, decision to publish, or preparation of the manuscript.

**Competing interests:** the authors have declared that no competing interests exist.

## 1. Introduction

Tumor development and reproduction were linked to increased vascularity (angiogenesis) in cancer cells, so the anti-angiogenesis mechanism was considered one of the potential strategies to fight cancer [1]. Vascular endothelial growth factor (VEGF) pathway was identified as a key regulator of angiogenesis. This fact was utilized in the discovery of outstanding numerous chemotherapeutic agents [2, 3]. Vascular endothelial growth factor receptors (VEGFRs) is the receptor of VEGF and include three subtypes (VEGFR-1, VEGFR-2, and VEGFR-3) [4].

The VEGFR-2 subtype is the most critical regulator of the angiogenesis process that plays a substantial role in the dissolution, migration, and proliferation of endothelial cells of cancer [5]. VEGFR-2 exerts its effect in cancer cells through binding to VEGF to boost the autophosphorylation process resulting in the motivation of a downstream signaling cascade that is essential for endothelial cell propagation and angiogenesis [6]. As a result, blocking the VEGF / VEGFR-2 system is a promising approach for the development of an anti-angiogenic therapy for slowing cancer growth [7, 8]. Furthermore, the antitumor effect of VEGFR-2 inhibitors have been enhanced by its ability to induce apoptosis [9–12].

Because of the nature of their large hydrophobic binding site, VEGFR-2 inhibitors have a wide range of structures [7]. However, the crystal structures of the two illustrious VEGFR-2 inhibitors (sorafenib and sunitinib) reveal common key interaction features that are essential for good fitting against VEGFR-2 (Fig 1). These features include primarily a flat heteroaromatic ring system for interaction with the hinge region including the focal amino acid Cys919 [8]. The second feature is a central linker to provide many  $\pi$ - $\pi$  interactions with Phe1047, Val916, Val848, and Cys1045 in the linker region [9]. The third feature includes a pharmacophore moiety which forms many hydrogen-bonds with the two key amino acids (Glu885 and Asp1046) in the DFG motif. The fourth feature includes hydrophobic moieties that extend to occupy the back hydrophobic pocket [10]. Chemoinformatics (*in silico* techniques) was used as an efficient approach in drug discovery with the advantage of saving time, effort, and costs [11–13]. This includes molecular docking [14, 15], ADMET assessment [15] and MD simulation techniques [14, 16].

In view of the above-mentioned findings and through our trip in the discovery of novel anticancer agents [17–20] especially VEGFR-2 inhibitors [21–28], our research group has paid much attention to develop a new series of anti-angiogenic candidates possessing the main features of sorafenib and sunitinib. Consequently, we used different bioisosteric moieties to occupy the main four regions of VEGFR-2 active pocket. In detail, for the hinge region, 3-oxoindoline and 2-oxo-1,2-dihydroquinolin were used as heteroaromatic moieties. The spacer (thiazolidine-2,4-dione) and pharmacophore (amide) moieties were targeted to occupy the gatekeeper and the DFG-motif regions, respectively. At last, the allosteric pocket was targeted by different aromatic structures (Fig 1). Moreover, all targeted products were subjected to deep biological studies including *in vitro* cytotoxic activities and VEGFR-2 inhibitory activity. Furthermore, the most promising member was further investigated for its apoptotic induction by assessing the gene expression of four genes (Bcl2, Bcl-xl, TGF, and Survivin). Further *in silico* studies including molecular docking, MD simulations, MM-PBSA, ADMET, and toxicity were conducted to correlate the affinity of our compounds against VEGFR-2.

## 2. Results and discussion

### 2.1. Chemistry

The target novel derivatives **10a-b** and **14a-c** were synthesized as depicted in Schemes 1 and 2. The starting materials **2** was prepared using the Vilsmeier-Haack reaction in which acetanilide

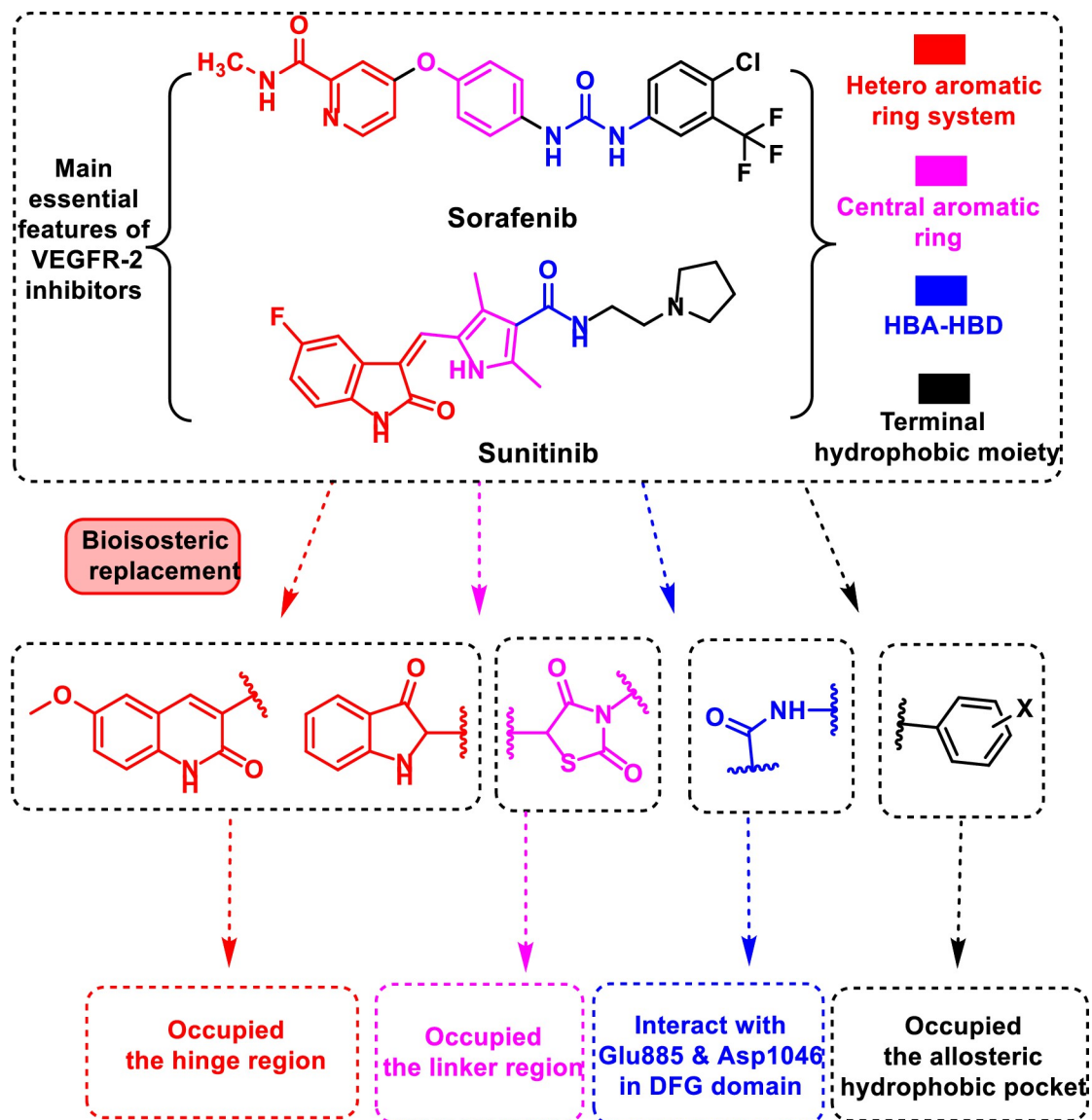
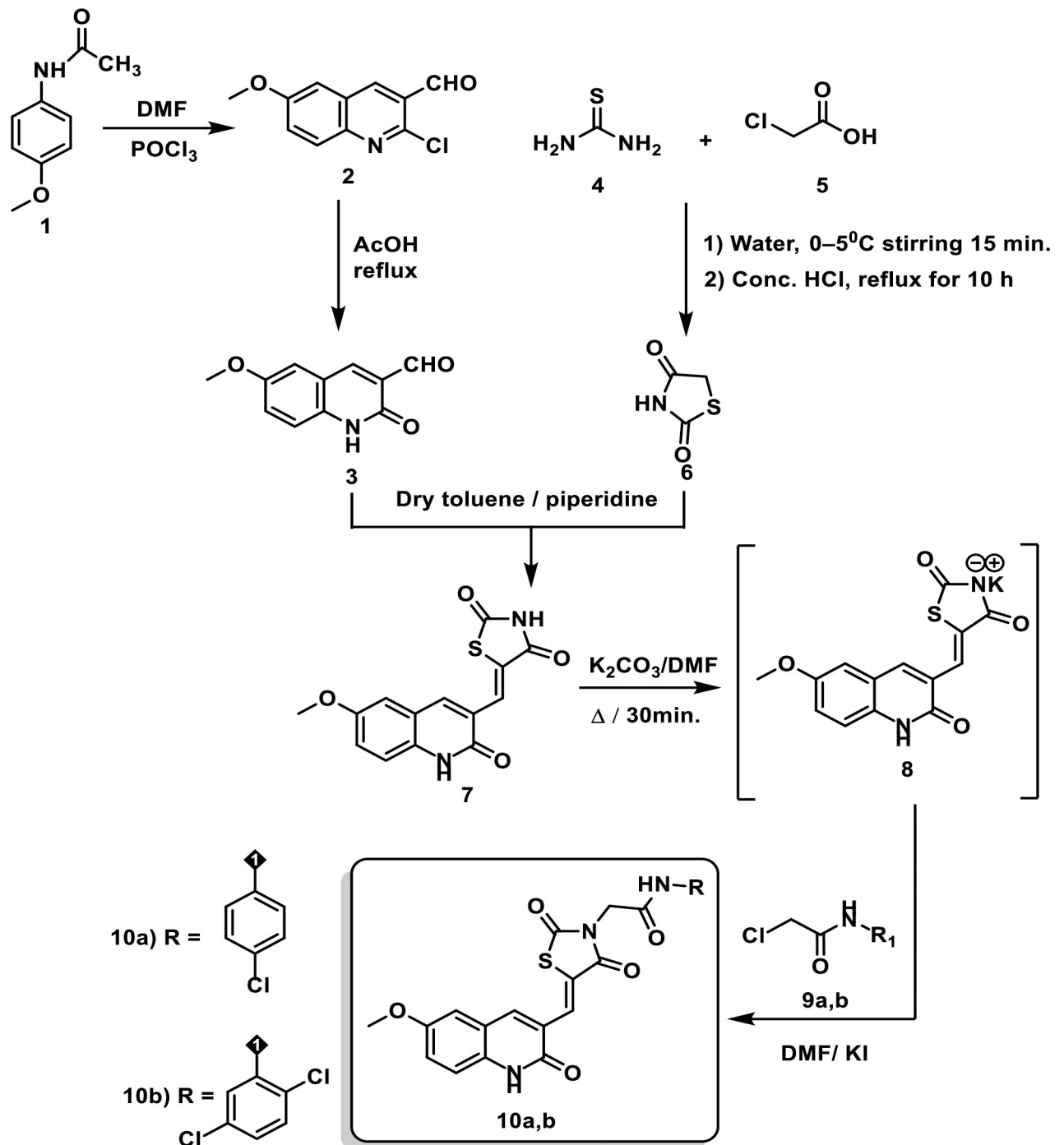


**Fig 1. The design rationale of proposed VEGFR-2 inhibitors.**

<https://doi.org/10.1371/journal.pone.0272362.g001>

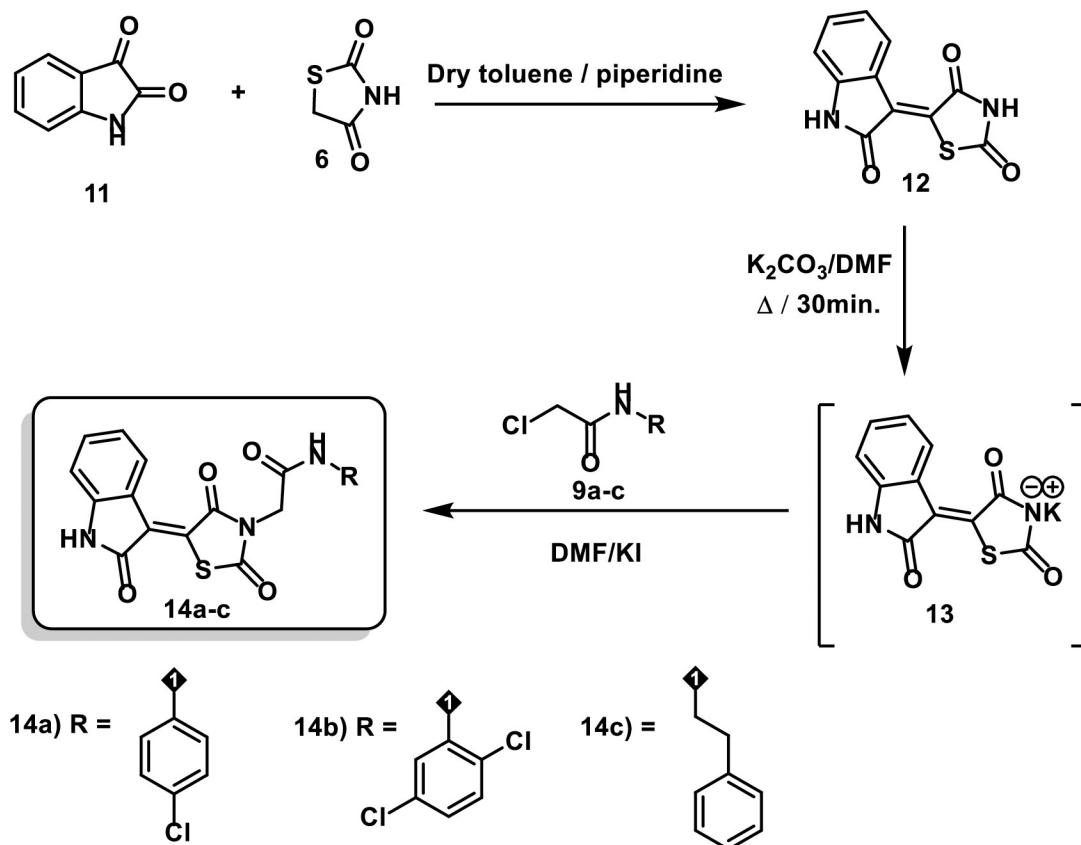
is converted into 2-chloroquinoline-3-carbaldehyde by the action of Vilsmeier-Haack reagent (DMF+POCl<sub>3</sub>) [29]. Next, compounds **3**, and **6** were prepared in high yields according to the literature procedures [30–34]. To prepare the key intermediate **7**, Knoevenagel condensation reaction was utilized [35]. In this reaction, quinoline **3** was condensed with thiazolidine-2,4-dione **6** in the presence of piperidine which acts as organocatalyst. In compound **7**, there are two NH groups, the thiazolidine NH group has a very strong acidic proton flanked by 2 carbonyl groups which stabilize the resulting anion produced after salt formation. Therefore, the thiazolidine NH group is involved in the salt formation rather than the quinoline NH group. Consequently, treatment of compounds **7** with dry K<sub>2</sub>CO<sub>3</sub> in DMF with continuous stirring afforded the corresponding *in situ* potassium salt **8**. Subsequent heating of potassium salt **8** with 2-chloro-*N*-substituted acetamide derivatives **9a, b** in dry DMF / KI mixture produced the corresponding desired compounds **10a, b**, respectively (Scheme 1).



Scheme 1. Synthesis of compounds 10a-b.

<https://doi.org/10.1371/journal.pone.0272362.g002>

On the other hand, compound **12** was prepared via condensation of thiazolidine-2,4-dione **6** with isatin **11** in a dry toluene/piperidine mixture following the reported procedures [34]. In compound **11**, the amide carbonyl is less electrophilic as it is stabilized by the lone pair of electrons of the nearby nitrogen atom. Therefore, the carbonyl in position 3 is more reactive and it is involved in the c-c bond formation with compound **6**. Treating compound **12** with dry



Scheme 2. Synthesis of compounds 14a-c.

<https://doi.org/10.1371/journal.pone.0272362.g003>

$\text{K}_2\text{CO}_3$  in DMF with continuous stirring afforded the corresponding *in situ* potassium salt **13**. Heating a mixture of compound **13** with 2-chloro-*N*-substitutedacetamide derivatives **9a-c** in dry DMF / KI mixture yielded the desired products **14a-c**, respectively (Scheme 2).

IR spectra of the target derivatives **10a-b** and **14a-c** confirmed their molecular structures by the presence of C = O bands ranging from 1673 to 1753  $\text{cm}^{-1}$  besides NH bands ranging from 3142 to 3449  $\text{cm}^{-1}$ . Concerning quinoline derivatives **10a-b**, singlet signals corresponding to the two amidic NHs were found in  $^1\text{H}$  NMR spectra around 10.65 and 10.24 ppm. With regard to the indoline derivatives **14a-c**, the structures of the obtained derivatives were supported by the generated spectral data. The  $^1\text{H}$  NMR spectra of compounds displayed singlet signals around 11.32 and 10.24 ppm for the NHs. Matching these findings,  $^{13}\text{C}$  NMR spectra displayed the characteristic peaks at the fingerprint regions.

## 2.2. Biological evaluation

**2.2.1. Assessment of *in vitro* anti-proliferative activity.** The cytotoxicity effects of the synthesized candidates were evaluated against A549, Caco-2, HepG2, and MDA-mb-231 cell lines. MTT assay method was applied using the sub- $\text{IC}_{50}$  concentrations of each compound as the treatment dose. Doxorubicin was used as a reference molecule. The obtained results demonstrated the anti-cancer effects of the tested compounds against all tested cell lines with different degrees (Table 1). Also, it was noticed that Caco-2 was the most sensitive cell line.

The most potent cytotoxic member was compound **14a**. It showed high cytotoxic effects against Caco-2 ( $\text{IC}_{50} = 1.5\mu\text{M}$ ) and HepG-2 ( $\text{IC}_{50} = 31.5\mu\text{M}$ ). Meanwhile, compound **10b**

Table 1. *In vitro* cytotoxicity against A549, Caco2, HepG2, and MDA-mb-231 cell lines.

| Comp.              | Anti-proliferative activity (IC <sub>50</sub> μM) |              |              |              |
|--------------------|---|--------------|--------------|--------------|
|                    | A549  | Caco2        | HepG2        | MDA-mb-231   |
| <b>10a</b>         | 85.0 ± 7.5  | 82.5 ± 7.2   | 173.5 ± 16.3 | 131.5 ± 5.2  |
| <b>10b</b>         | 92.5 ± 8.6  | 62.5 ± 5.4   | 71.0 ± 6.4   | 31.5 ± 2.5   |
| <b>14a</b>         | 170.0 ± 14.5                                      | 1.5 ± 0.08   | 31.5 ± 2.5   | 84.0 ± 7.3   |
| <b>14b</b>         | 292.5 ± 25.1                                      | 74.0 ± 6.5   | 42.5 ± 3.2   | 94.5 ± 8.4   |
| <b>14c</b>         | 281.5 ± 27.3                                      | 192.5 ± 18.1 | 92.0 ± 8.1   | 484 ± 47.2   |
| <b>Doxorubicin</b> | 86.44 ± 7.1                                       | 3.5 ± 0.22   | 1.2 ± 0.07   | 0.98 ± 0.001 |

<https://doi.org/10.1371/journal.pone.0272362.t001>

came in the second order as it showed moderate anticancer effect against MDA mb-231 cell line (IC<sub>50</sub> = 31.5 μM) and Caco-2 (IC<sub>50</sub> = 62.5 μM). Regarding A549 cell line, compound **10a** displayed the most potent cytotoxic activity (IC<sub>50</sub> = 85 μM).

**2.2.2. Assessment of VEGFR-2 inhibition.** Compounds **10a**, **b** and **14a-c** were evaluated for their VEGFR-2 inhibitory activity. Sorafenib (the reference drug) produced IC<sub>50</sub> value of 53.65 nM (Table 2). The quinoline derivative **10a** (IC<sub>50</sub> = 65.16 nM) is the most active member compared to sorafenib. Concerning the indoline derivatives **14a-c**, it was found that different hydrophobic tails gave valuable SAR. In detail, compound **14c** (IC<sub>50</sub> = 81.46 nM) incorporating phenethyl moiety as a hydrophobic tail was the most active indoline member. This revealed that the terminal aliphatic moieties have the highest positive effect on VEGFR-2 inhibition. Shifting the hydrophobic tail into aromatic moieties as in compounds **14a** (incorporating 4-chlorophenyl moiety, IC<sub>50</sub> = 91.51 nM) and **14b** (incorporating 2,4-dichlorophenyl moiety, IC<sub>50</sub> = 85.85 nM) led to a slight decrease in the VEGFR-2 inhibitory activity.

**2.2.3. Safety pattern of the tested compounds.** In this work, the safety pattern of the synthesized derivatives **10a**, **b** and **14a-c** was also evaluated by testing their *in vitro* cytotoxicity against Vero non-cancer cell line using the MTT assay protocol. The obtained results showed an IC<sub>50</sub> range of 194–1580 μM presenting the safety profile of the examined hits against the Vero normal cell line. Compounds **10b** (IC<sub>50</sub> = 1580 μM) and **14b** (IC<sub>50</sub> = 1270 μM) were the safest members (Table 3).

**2.2.4. Selectivity index (SI).** To clinch the cyto-protective properties of the compounds, the drug safety parameter for anticancer activity of the compounds was estimated by comparing their cytotoxic effect against tumor cell lines and normal cell lines. The normal human Vero cell line was used as a control in this study. Table 4 shows the calculated SI for the tested compounds by scaling its IC<sub>50</sub> value against various tumor cell lines and IC<sub>50</sub> value against a normal cell line (Vero cell line) [36]. When the SI value of a compound is ≥10 then it is considered a selective anticancer agent [37].

As previously stated in the former test, all the tested derivatives had lower potency against Vero cell lines. These outcomes prompted us to investigate the selectivity profile of the

Table 2. Inhibitory effects of compounds 10a, b and 14a-c against VEGFR-2.

| Comp.            | VEGFR-2 IC <sub>50</sub> (nM) |
|------------------|-------------------------------|
| <b>10a</b>       | 65.16 ± 5.5                   |
| <b>10b</b>       | 164.5 ± 15.3                  |
| <b>14a</b>       | 91.51 ± 8.2                   |
| <b>14b</b>       | 85.85 ± 7.6                   |
| <b>14c</b>       | 81.46 ± 7.3                   |
| <b>Sorafenib</b> | ± 4.5                         |

<https://doi.org/10.1371/journal.pone.0272362.t002>

**Table 3. IC<sub>50</sub> results of 10a, b and 14a-c against Vero cell line.**

| Compound No. | Cytotoxicity against Vero (IC <sub>50</sub> μM) |
|--------------|---|
| <b>10a</b>   | 194 ± 18.2                                      |
| <b>10b</b>   | 1580 ± 155.1                                    |
| <b>14a</b>   | 290 ± 28.3                                      |
| <b>14b</b>   | 1270 ± 126.5                                    |
| <b>14c</b>   | 1. ± 96.6                                       |

<https://doi.org/10.1371/journal.pone.0272362.t003>

synthesized compounds by calculating selectivity index value for each compound against the four cancer cells. The maximum selectivity index value was recorded for **14a** (212.5) against Caco-2 cell lines as displayed in Fig 2. Therefore, compound **14a** was decided to be the safest potent member of synthesized compounds and was nominated for further biological testing.

**2.2.5. Effect of compound 14a on Caco-2 cells migration.** The *in vitro* scratch assay [38] was used to assess the prospective of compound **14a** to inhibit the ability of Caco-2 cells to migrate and heal. The basic idea behind this test is to create a scratch in a cancer cell line monolayer, measure the diameter at the start time and at regular intervals to investigate the potential of the cancer cell to migrate and heal. The findings of the treated cell line are then compared to the untreated cell line. Fig 3 shows images of scratched areas at time points 0 and 24.

The obtained findings revealed that the scratch of the untreated cells was completely closed within 24 h (Fig 3B). On the other hand, the width of the scratch in Caco-2 cell lines that were treated with **14a** (1 μM) slightly decreased from the control cells' scratch width at 0 hr (0.356 to 0.293 mm) as displayed in Fig 3A and 3C. These findings confirmed that even at a low concentration of 1 μM, compound **14a** can inhibit the migration and healing of Caco-2 cells in a significant manner. Also, at the end of the 24-hour incubation period, compound **14a** was able to make a significant phenotypic change in cancer cell morphology which might be linked to the occurrence of apoptosis.

**2.2.6. Alternation of cancer cells gene expression after Caco-2 treatment with 14a using RT-qPCR.** The apoptosis process (programmed cell death) is mediated by different gene families such as caspases, tumor necrosis factor (TNF) receptor gene superfamily, or B cell lymphoma (Bcl)-2 family. Survivin is a pro-survival protein that is overexpressed in many cancer cells in the G2-M phase. This protein has been linked to tumor progression control and resistance to cancer chemotherapeutics. Furthermore, the transforming growth factor (TGF)

**Table 4. Selectivity indices of the synthesized compounds.**

| Compounds  | (A549) <sup>a</sup> | (Caco-2) <sup>b</sup> | (HepG2) <sup>c</sup> | (MDA-MB-231) <sup>d</sup> |
|------------|---------------------|-----------------------|----------------------|---------------------------|
| <b>10a</b> | 2.280               | 2.352                 | 1.118                | 1.460                     |
| <b>10b</b> | 17.080              | 25.290                | 22.250               | 51.333                    |
| <b>14a</b> | 1.704               | 212.500               | 9.196                | 3.375                     |
| <b>14b</b> | 4.340               | 17.150                | 29.917               | 13.555                    |
| <b>14c</b> | 3.463               | 5.0654                | 10.601               | 2.020                     |

<sup>a</sup> SI = Cytotoxicity against Vero cells / Cytotoxicity against A549 cell line.

<sup>b</sup> SI = Cytotoxicity against Vero cells / Cytotoxicity against Caco-2 cell line.

<sup>c</sup> SI = Cytotoxicity against Vero cells / Cytotoxicity against HepG2 cell line.

<sup>d</sup> SI = Cytotoxicity against Vero cells / Cytotoxicity against MDA-MB-231 cell line.

<https://doi.org/10.1371/journal.pone.0272362.t004>

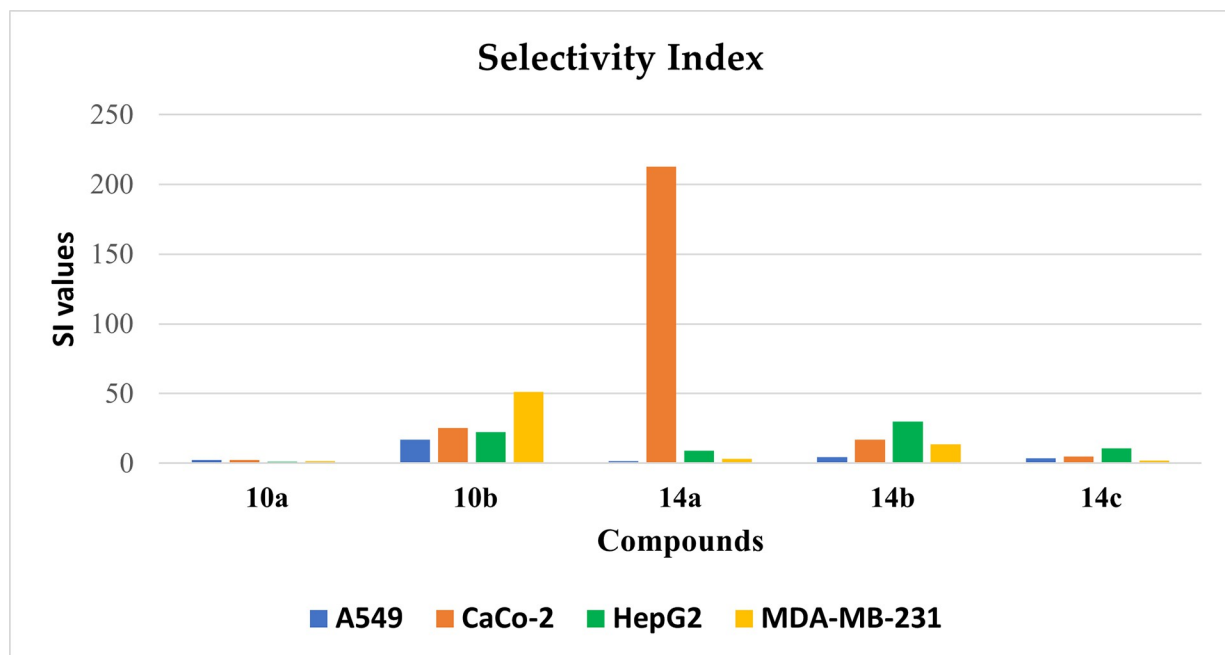


**Fig 2. Selectivity indices of the synthesized compounds.**

<https://doi.org/10.1371/journal.pone.0272362.g004>

is a key protein that can promote the development of normal cells and participate in the suppression mechanism of tumor cells [39]. Dysregulation of TGF- $\beta$  activation and signaling may result in apoptosis. Moreover, overexpression of the Bcl2 gene can inhibit apoptosis. Meanwhile, overexpression of Bcl-xL enhances autophagic cell death [40].

In this study, the Caco-2 cell line was treated with 1.5  $\mu$ M (IC<sub>50</sub> value) of compound **14a**. The results showed noticeable variations in the expression levels of the four cancer correlated genes (Bcl-2, Bcl-xL, TGF, and Survivin). In detail, compared to control cells, compound **14a** caused significant down-regulation of Bcl-2, and Survivin and TGF gene expression levels. Meanwhile, the gene expression level of Bcl-xL showed non-detectable change. These findings indicate the efficiency of compound **14a** in the induction of apoptosis (Fig 4).

### 2.3. *In silico* studies

**2.3.1. Molecular docking.** The docking studies can give a good insight about the binding modes of many active molecules [41–43]. These studies aimed to determine the binding modes and orientation of the designed VEGFR2 kinase inhibitors. In the present work, the crystal structure of VEGFR2 (PDB code 4ASD) was retrieved from the protein data bank. The docking protocol was initially validated by re-docking of the co-crystallized ligand (sorafenib) into the active site of VEGFR 2. The respective validation criteria in this study showed an RMSD value = 1.15 Å, and a docking score = -11.25 kcal/mole.

As presented in Fig 5, the docking pose of sorafenib involved three H-bonding with Cys919, Glu885, and Asp1046. Also, it interacted with the hydrophobic pocket formed by Leu889, Leu1019, and Ile892 via several hydrophobic interactions.

Compound **10a** occupied the hinge region via its 2-oxoquinoline moiety. It formed a hydrogen bond with Cys919 and eight hydrophobic interactions with Cys919, Leu840, Leu1035, Ala866, and Phe918. Next, the thiazolidine-2,4-dione moiety was incorporated in the linker region via the formation of five pi-pi interactions with Val916, Val848, Val899, Ala866,

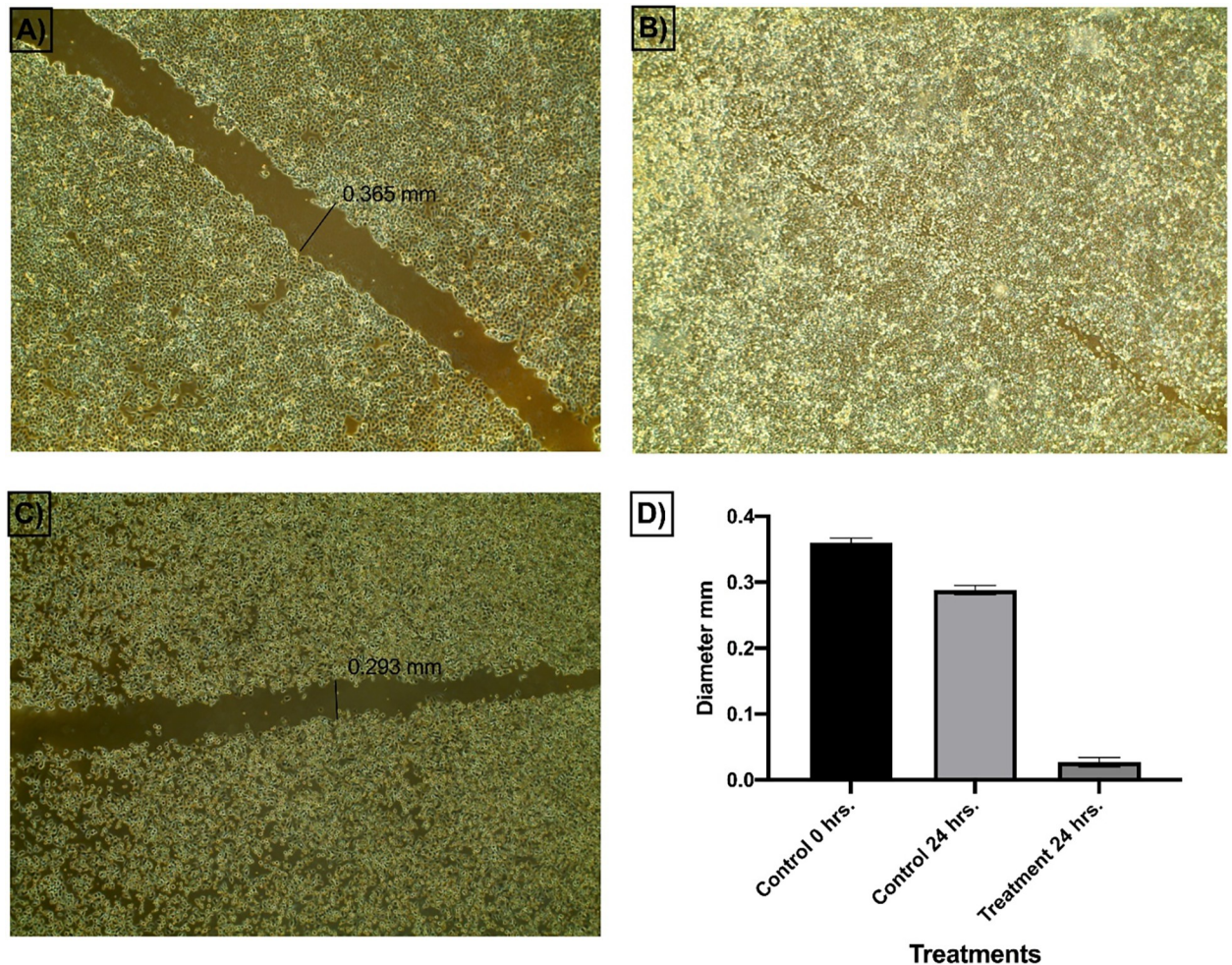


**Fig 3.** Effect of compound 14a on cells migration and healing efficacy of Caco-2 cells.

<https://doi.org/10.1371/journal.pone.0272362.g005>

and Lys868. In addition, it formed one hydrogen bond with Asp1046. As well, the amide moiety was buried in the DFG motif region to form two H bonds with Asp1046 and Glu885. Lastly, the *p*-chlorophenyl group achieved one hydrophobic interaction with Leu889 in the hydrophobic back pocket (Fig 6).

The docking findings of compound 14a, the most promising member in this study, revealed similar binding pattern with sorafenib. The 2-oxoindolin moiety was oriented toward the hinge region forming one H bond interaction with Glu917 residue and seven hydrophobic interactions with, Leu840, Leu1035, Ala866, Phe918, and the key amino acid Cys919. Meanwhile, the thiazolidine-2,4-dione moiety was accommodated in the linker region to form five hydrophobic interactions with Val916, Val848, Ala866, Phe1047, and Cys1045. Similarly, compound 14a interacted *via* one H-bond with Glu885 (1.80 Å) and another one with Asp1046 (2.02 Å) of the conserved DFG motif region. Finally, one hydrophobic interaction was observed between compound 14a and hydrophobic side chains of Leu899 in the hydrophobic back pocket of VEGFR-2 (Fig 7). The binding modes of compounds were presented in S.2.1.1 and S2.1.2. Sections in S1 File.

The docked pose of compound 14b was depicted in Fig 8. The amide group formed two hydrogen bonds with Glu885 (COO<sup>-</sup>, 1.65 Å) and Asp1046 (NH, 2.04 Å). Moreover, it formed

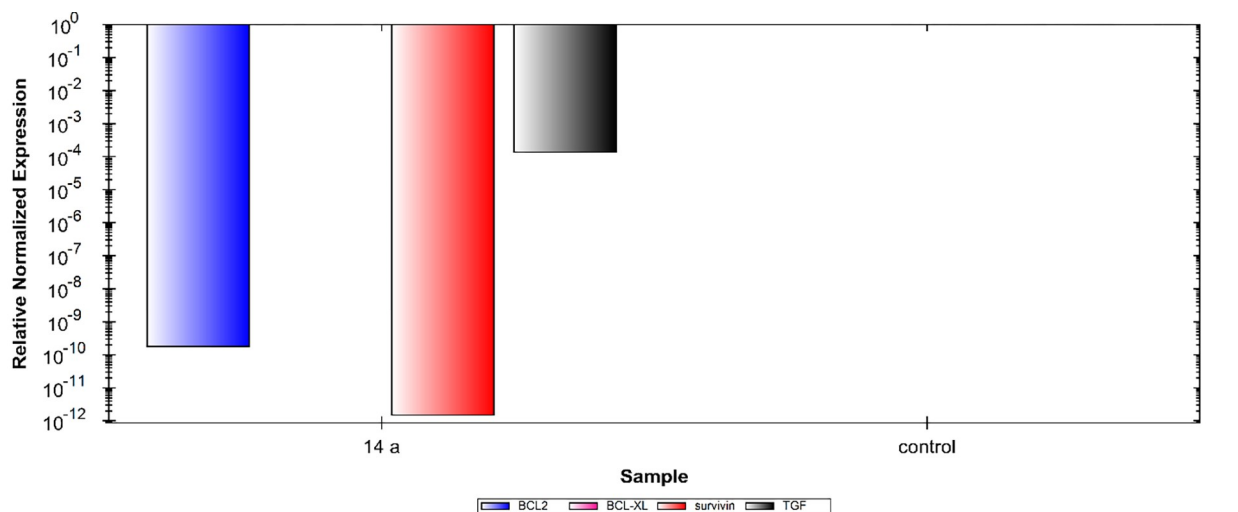


**Fig 4.** Relative gene expression levels of 4 different genes (Bcl-2, Bcl-xl, Survivin, and TGF) in Caco-2 cell line treated with 14a using RT-qPCR.

<https://doi.org/10.1371/journal.pone.0272362.g006>

four hydrophobic interactions in the linker region with Val916, Val848, Phe1047, and Cys1045 via its thiazolidine-2,4-dione moiety. As well, the 2-oxindolin moiety was buried in the hinge region forming one H bond interaction with Glu917 besides several hydrophobic interactions with Leu840, Leu1035, Ala866, Val848, and Cys919. Moreover, the 2,5-dichlorophenyl moiety formed four hydrophobic interactions with Leu899, Ile1044, Leu1019, and Val898 in the allosteric hydrophobic pocket.

**2.3.2. Flexible alignment study.** In this test, 3D- flexible alignment of compound **14a** (the most promising member) with sorafenib was carried out. The results revealed a general good overlap of compound **14a** with sorafenib with the same spatial orientation. In details, 2-oxindolin, thiazolidine-2,4-dione, amide, and 4-chlorophenyl moieties of compound **14a** showed the same orientation of the *N*-methylpicolinamide, phenoxy, urea, and 4-chloro-3-(trifluoromethyl)phenyl moieties of sorafenib, respectively (Fig 9A and 9B). This study revealed that compound **14a** has the same basic pharmacophoric features of sorafenib and can occupy the VEGFR-2 kinase active pocket with the same orientation of sorafenib as displayed in (Fig 9C).

**2.3.3. ADMET profiling study.** The pharmacokinetic properties were determined computationally for compounds **10a**, **b** and **14a-c** using Discovery studio 4.0 (Fig 10). Sorafenib and sunitinib were used as references.

As shown in Table 5, compounds **10a-b** and **14a-c** achieved good absorption levels upon oral administration. Moreover, the titled compounds could exhibit acceptable BBB penetration levels. Finally, all compounds showed a theoretical non-inhibitory effect against CYP2D6 with plasma protein binding ability than 90%.

**2.3.4. In silico toxicity studies.** Toxicity profiles were computed for the tested derivatives **10a-b** and **14a-c** against references (sorafenib and sunitinib) based on seven constructed toxicity models created in Discovery studio software [44, 45] as presented in Table 6.

All the tested molecules were predicted as non-carcinogenic. In addition, all members except **10b** and **14b** had carcinogenic potency TD<sub>50</sub> values ranging from 14.284 to 121.482 mg/kg body weight/day, which were higher than that of sorafenib and sunitinib (14.244, 4.134 mg/kg body weight/day, respectively). In addition, all members had rat maximum tolerated doses lower than that of sorafenib and sunitinib. For the rat oral LD<sub>50</sub> model, compounds **10a**, **14a** and **12c** displayed oral LD<sub>50</sub> values of 0.936, 1.667 and 1.933 mg/kg body weight/day. Such

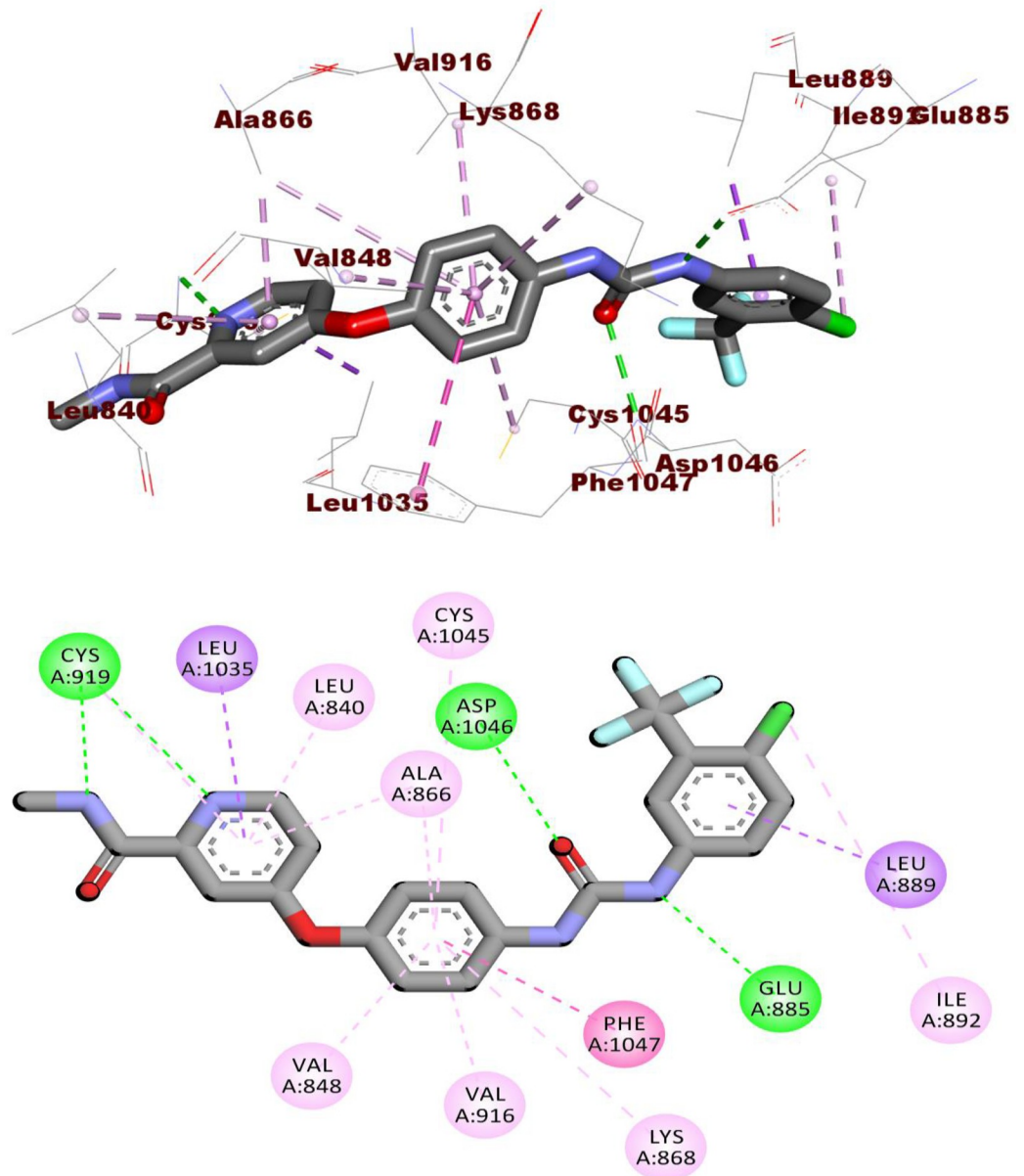


**Fig 5.** The docked pose of sorafenib against VEGFR-2.

<https://doi.org/10.1371/journal.pone.0272362.g007>

values are far more than that of sorafenib (0.823 mg/kg body weight/day). Also, all compounds except **10a** and **10b** showed rat chronic LOAEL values ranging from 0.030 to 0.069 which were higher than that of sorafenib (0.005). Finally, all candidates showed mild irritancy against eye with non-irritancy against skin.

**2.3.5. Molecular dynamics simulations.** The application of Molecular dynamics (MD) simulations is closely to be a regular *in silico* method in the area of drug development and discovery [46]. The main benefit of these types of work is the extreme accuracy in the analysis of every structural and entropic variation in the considered compound-protein system. Moreover, this experiment occurred at a very accurate atomic resolution through a given time [47]. Respectively, MD simulations can precisely calculate the resulted variations after the compound-protein binding in thermodynamic as well as kinetic levels [48]. These advantages

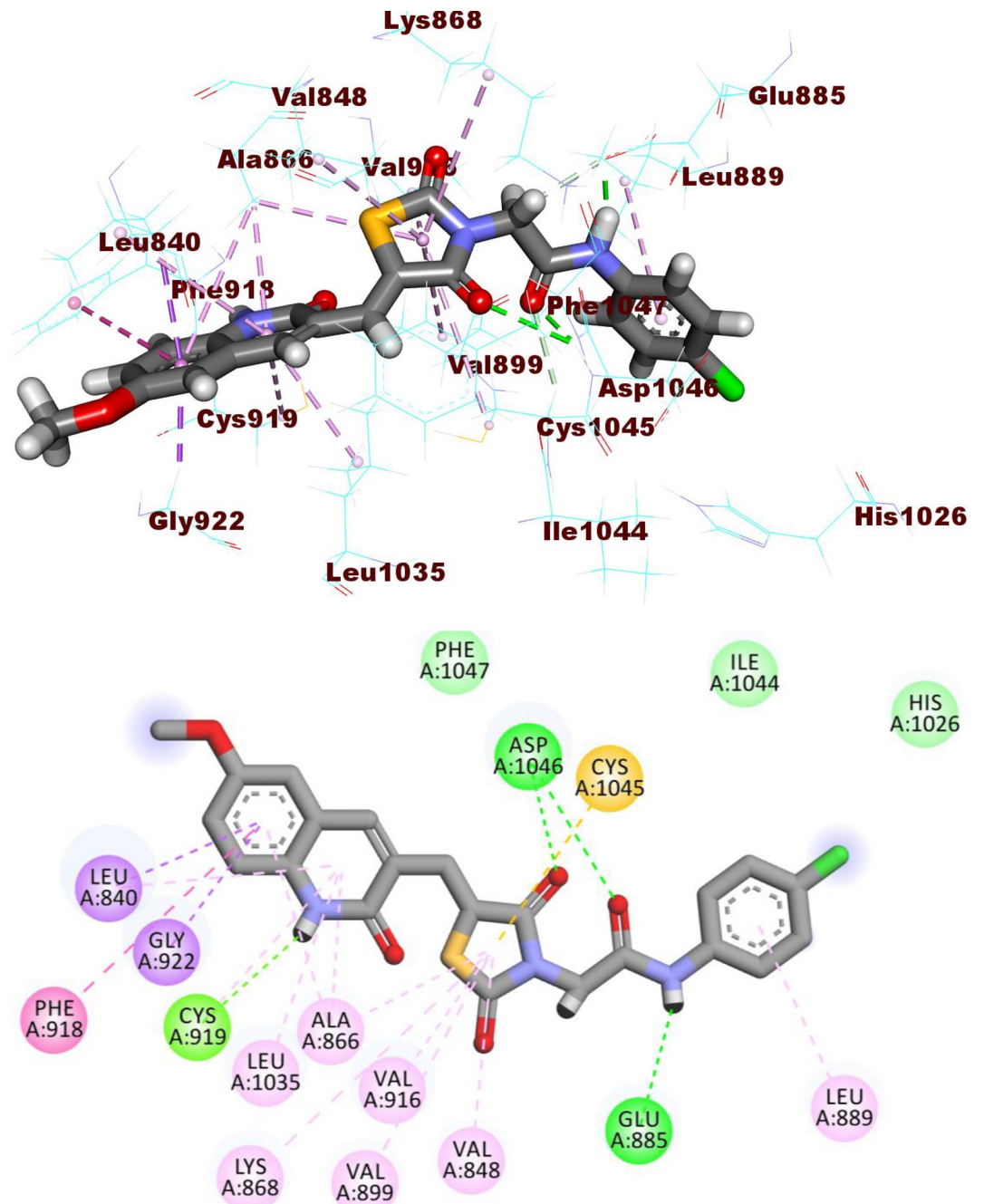


**Fig 6.** The docked pose of 10a against VEGFR-2.

<https://doi.org/10.1371/journal.pone.0272362.g008>

presented the MD as a successful tool to explain the structure-functional changes of the considered compound-protein complex. It reveals essential features such as stability, binding energy, and the kinetics of the examined complex [49].

To identify the conformational alterations that transpired in the VEGFR-2-14a complex because of binding, RMSD values were measured before and after 14a binding with the VEGFR-2. Fig 11A illustrates that VEGFR-2, 14a, and the VEGFR-2-14a complex had low RMSD values and didn't reveal major fluctuations during the MD time (100ns). These results

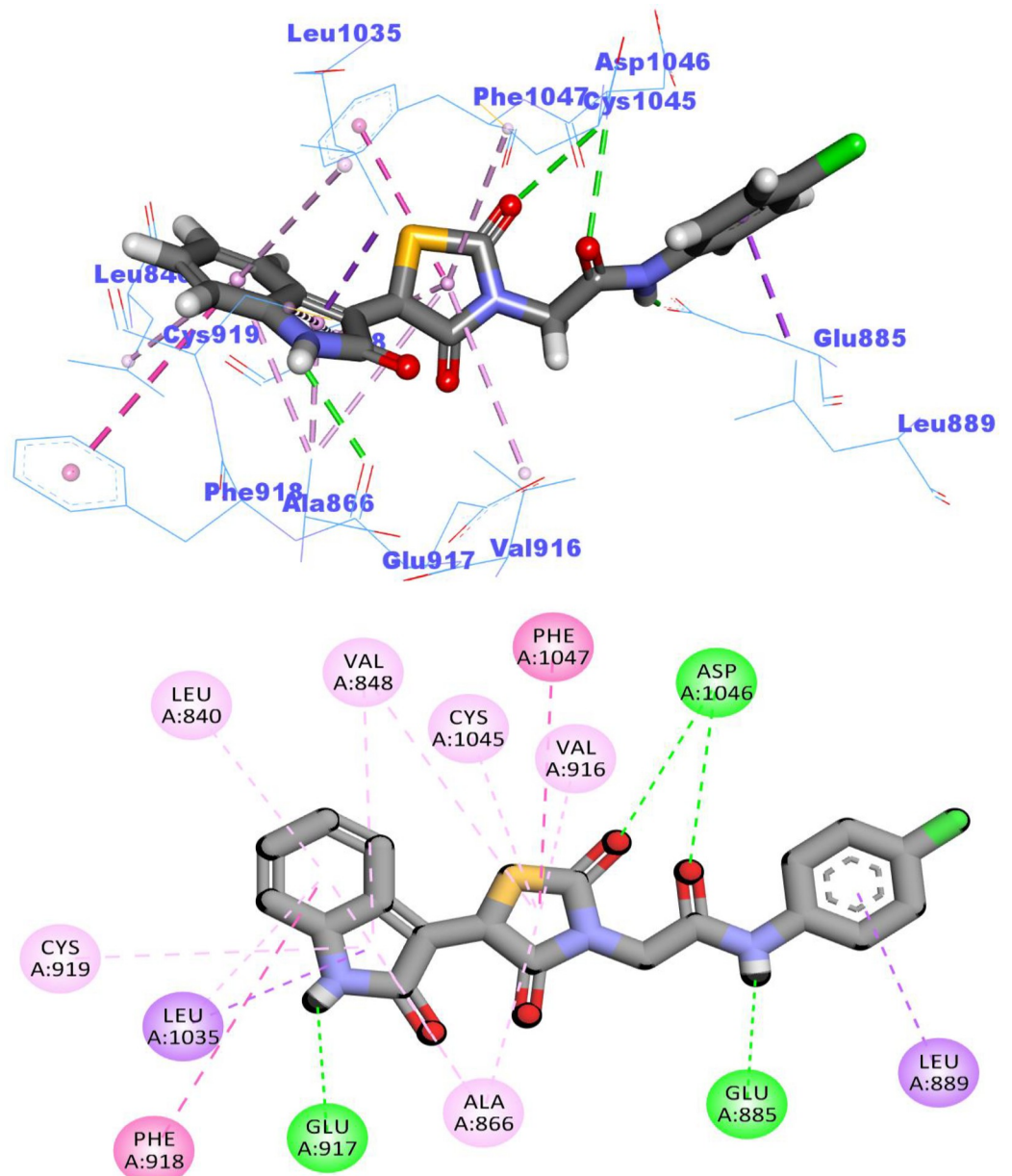


**Fig 7. The docked pose of 14a against VEGFR-2.**

<https://doi.org/10.1371/journal.pone.0272362.g009>

declare a high stability. The flexibility of VEGFR-2 enzyme after binding was checked in terms of RMSF to identify the fluctuated regions during 100 ns of simulation. Fortunately, **14a** didn't make the VEGFR-2 flexible (**Fig 11B**) after binding comparing the apo state of VEGFR-2 (**Fig 12A**). The radius of gyration ( $R_g$ ) of the enzyme VEGFR-2 was computed to explore the compactness of the examined VEGFR-2-**14a** system. Interestingly, the  $R_g$  of the VEGFR-2-**14a** complex remained stable till the end of the experiment (**Fig 11C**) and was not very distinct to that of VEGFR-2 apo state (**Fig 12B**). VEGFR-2-**14a** complex interaction against the solvents in the surrounding media was examined by solvent accessible surface area (SASA) over a period of 100 ns. Excitingly, VEGFR-2 enzyme didn't exhibit a noticeable expansion nor reduction of the surface area revealing nearly similar SASA values from 0 till 100 ns (**Fig 11D**).

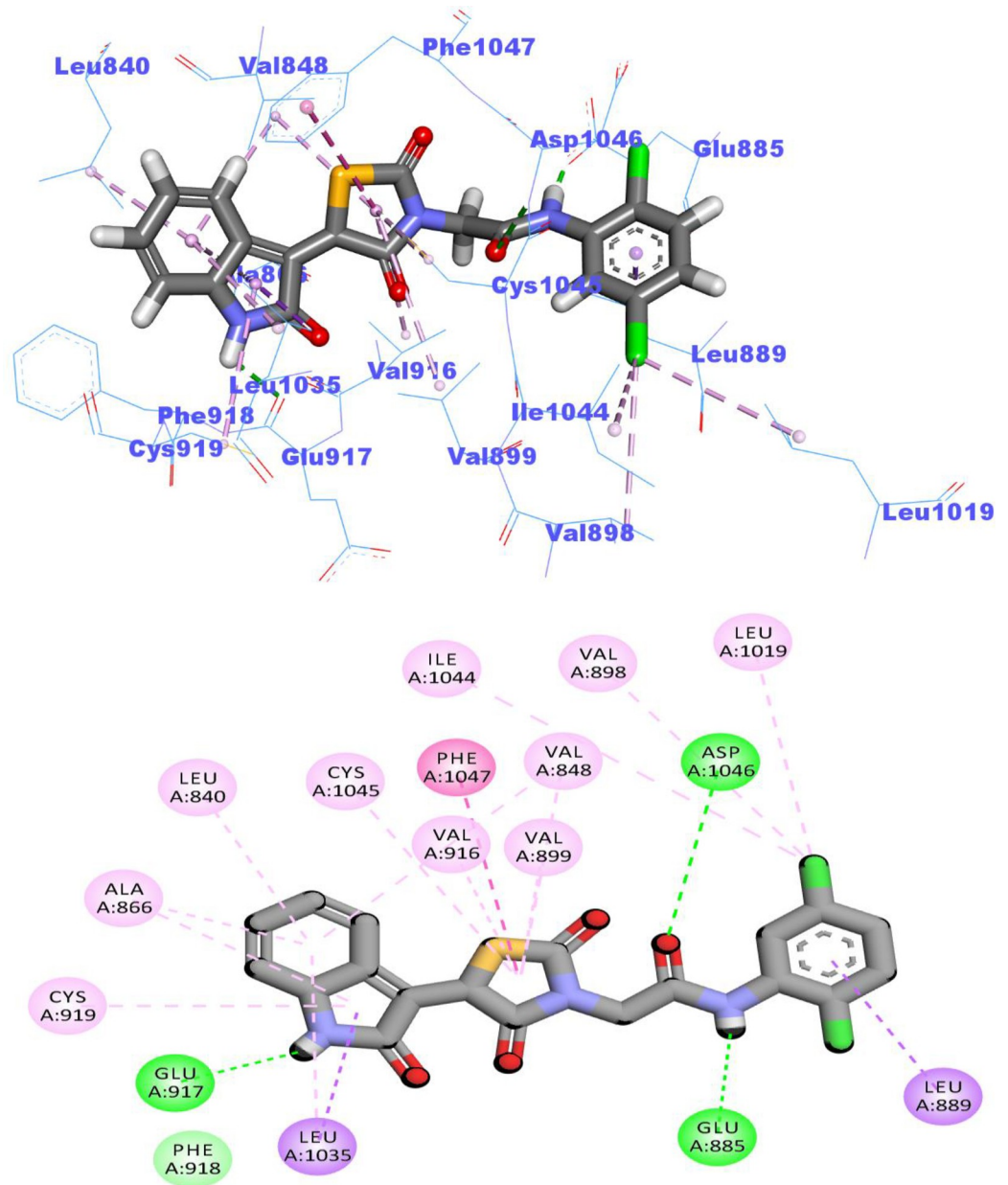


**Fig 8.** The docked pose of 14b against VEGFR-2.

<https://doi.org/10.1371/journal.pone.0272362.g010>

The obtained values were near to that of VEGFR-2 apo state (Fig 12C) indicating that there is no major conformational alternations occurred in VEGFR-2 enzyme due to 14a binding. Also, hydrogen bonding in the VEGFR-2-14a complex was computed and the maximum incorporated H-bonds number was found to be three (Fig 11E).

To understand the conformational changes that was reported in the RMSD study, the conformational change analysis of the 14a-VEGFR-2 complex was analyzed during the 1, and 100 ns of the MD production run as illustrated in Fig 13. The conformational changes in VEGFR-2 were indicated. Most importantly, the binding stability as well as the integrity of the 14a-VEGFR-2 complex was confirmed.

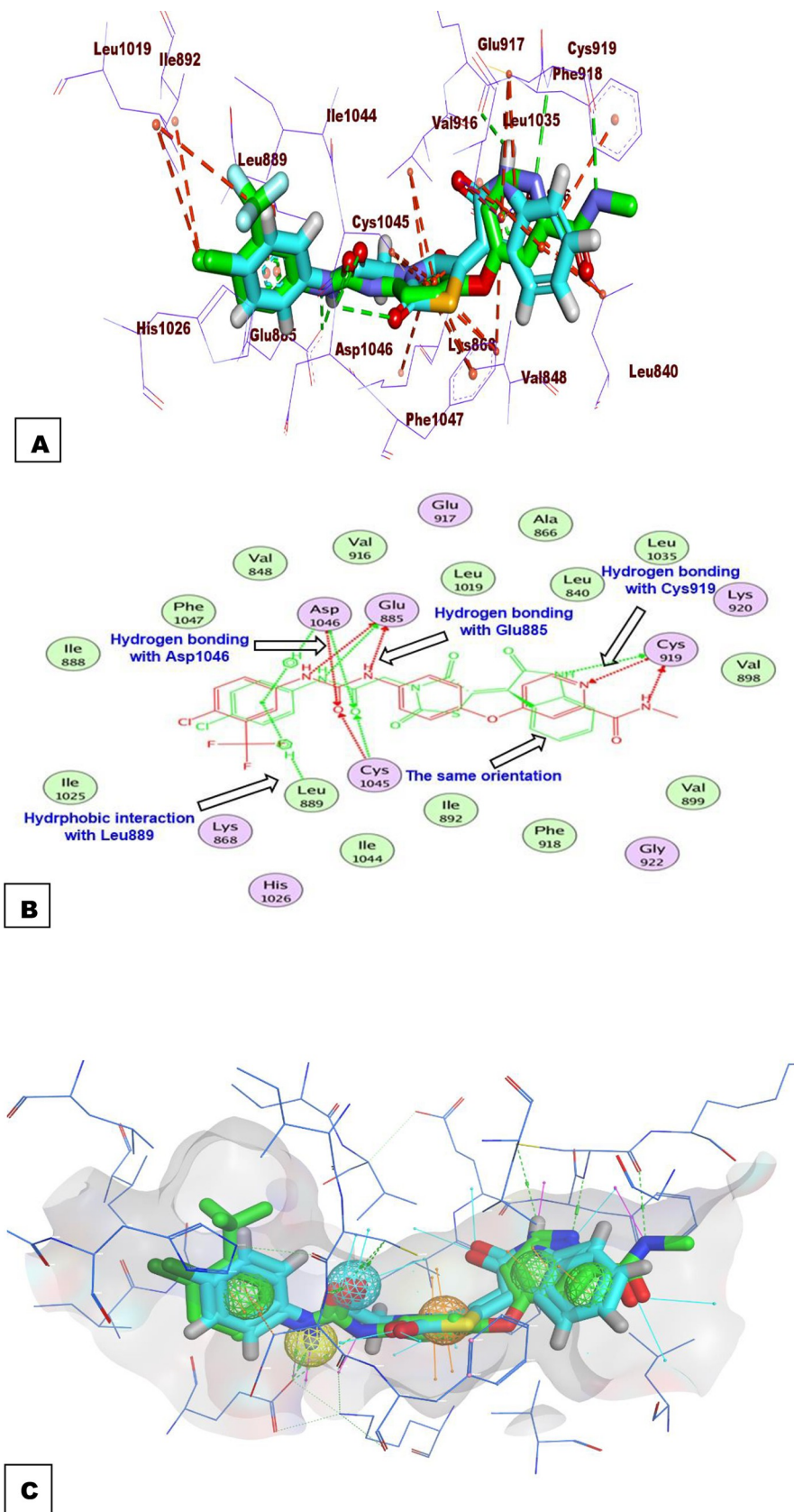


**Fig 9. Orientation compound 14a and sorafenib inside the active sites of VEGFR-2.**

<https://doi.org/10.1371/journal.pone.0272362.g011>

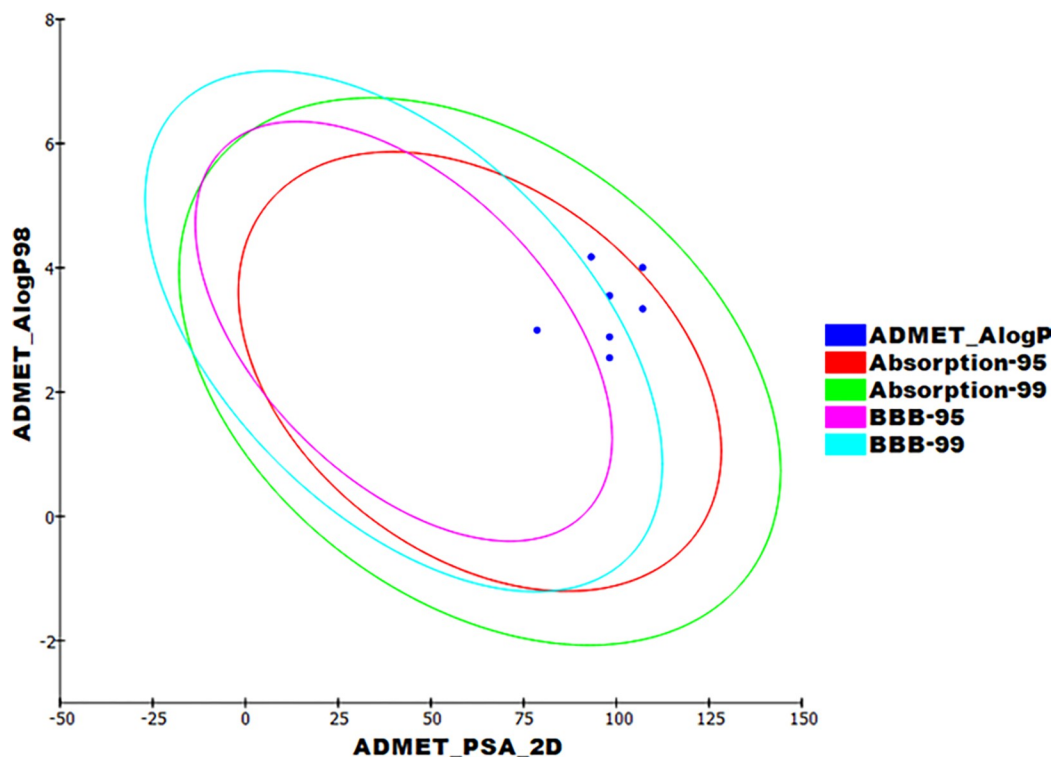


Fig 10. Theoretical ADMET characters.

<https://doi.org/10.1371/journal.pone.0272362.g012>

**2.3.5.1. MM/PBSA studies.** The binding free energy of **14a**-VEGFR-2 system was computed the last 20 ns of the obtained MD production with a 100 ps interval from the MD trajectories using. Compound **14a** exhibited a binding free energy of -75 KJ/mol with VEGFR-2 enzyme (Fig 14A). Moreover, the participation of each individual residue in the binding free energy of **14a**-VEGFR-2 system were disclosed. The total binding free energy of the **14a**-VEGFR-2 system was disintegrated into per individual residue energy. The output of this experiment sheds a light into the pivotal amino acid residues that contributed remarkably to the binding of **14a**

Table 5. Different theoretical ADMET characters of the tested compounds.

| Comp.     | BBB <sup>a</sup> | Solubility <sup>b</sup> | Absorption <sup>c</sup> | CYP2D6 <sup>d</sup> | PPB <sup>e</sup> |
|-----------|------------------|-------------------------|-------------------------|---------------------|------------------|
| 10a       | ■■■■             | ■■                      | ⊗                       | ⊗                   | ✓                |
| 10b       | ■■■■             | ■■                      | ■                       | ⊗                   | ✓                |
| 14a       | ■■■              | ■■                      | ⊗                       | ⊗                   | ✓                |
| 14b       | ■■■■             | ■■                      | ⊗                       | ⊗                   | ✓                |
| 14c       | ■■■              | ■■                      | ⊗                       | ⊗                   | ✓                |
| Sorafenib | ■■■■             | ■                       | ⊗                       | ⊗                   | ✓                |
| Sunitinib | ■■               | ■■                      | ⊗                       | ⊗                   | ⊗                |

<sup>a</sup>BBB level, blood brain barrier level, ⊗ = very high, ■ = high, ■■ = medium, ■■■ = low, ■■■■ = very low.

<sup>b</sup>Solubility level, ■ = very low, ■■ = low, ■■■ = good, ■■■■ = optimal.

<sup>c</sup>Absorption level, ⊗ = good, ■ = moderate, ■■ = poor, ■■■ = very poor.

<sup>d</sup>CYP2D6, cytochrome P2D6, ✓ = inhibitor, ⊗ = non inhibitor.

<sup>e</sup>PBB, plasma protein binding, ⊗ means less than 90%, ✓ means more than 90%

<https://doi.org/10.1371/journal.pone.0272362.t005>

Table 6. *In silico* toxicity studies.

| Comp.     | Carcinogenicity <sup>a</sup> | Carcinogenic Potency TD <sub>50</sub><br>(mg/kg body weight/day) | Rat Maximum Tolerated<br>Dose (g/kg body weight) | Rat Oral LD <sub>50</sub> (g/<br>kg body weight) | Rat Chronic LOAEL<br>(g/kg body weight) | Ocular<br>Irritancy <sup>b</sup> | Skin<br>Irritancy <sup>b</sup> |
|-----------|------------------------------|--|--|--|---|----------------------------------|--------------------------------|
| 10a       | ☒                            | 15.044   | 0.026  | 0.936  | 0.002                                   | ✓                                | ☒                              |
| 10b       | ☒                            | 13.611   | 0.021  | 0.316  | 0.002                                   | ✓                                | ☒                              |
| 14a       | ☒                            | 14.284   | 0.059  | 1.667  | 0.030                                   | ✓                                | ☒                              |
| 14b       | ☒                            | 13.040   | 0.048  | 0.707  | 0.028                                   | ✓                                | ☒                              |
| 14c       | ☒                            | 121.482  | 0.042  | 1.933  | 0.069                                   | ✓                                | ☒                              |
| Sorafenib | ☒                            | 14.244   | 0.089  | 0.823  | 0.005                                   | ✓                                | ☒                              |
| Sunitinib | ☒                            | 4.134  | 0.178  | 2.876  | 0.040                                   | ✓                                | ☒                              |

<sup>a</sup> Carcinogenicity: ☒ = non-carcinogenic, ✓ = carcinogenic

<sup>b</sup> skin and ocular irritancy = ☒ = non-irritant, ✓ = irritant

<https://doi.org/10.1371/journal.pone.0272362.t006>

and VEGFR-2. The following amino acids: VAL-848, LEU-889, LEU-1035 and CYS-1045 of VEGFR-2 shared more than -5 KJ/mol binding energy and considered as hotspots in the binding with **14a** (Fig 14B).

**2.3.6. Density Function Theory (DFT) calculations.** The enzymatic inhibitory activity of targeted compounds against VEGFR-2 showed that the indoline derivative **14a** was the most active compound as incorporating 4-chlorophenyl moiety raised the IC<sub>50</sub> to 91.51 nM, Table 2. As discussed before, the **14a** derivative was produced from the reaction of **9a** with **13**. The reactivity and stability of formed **14a** will be highlighted from the point of view of DFT calculations. The Molecular electrostatic potential map (MEP) will be discussed as well. The DFT (B3LYP) method with 6-311G++(d,p) basis set to optimize organic structure compounds. Both TDOS and MEP were performed at the same level of theory.

The full optimized structure of **14a**, **9a** and **13** are shown in Fig 15. The obtained total energy of **14a** system was -55925.2 eV which is higher than those of free systems **13** and **9a**, -47778.3 and -36986.6 eV, respectively. The dipole moment for the **14a** was found to be 8.11 Debye (higher than those of free components, **13**; 7.6 Debye; and **9a**; 2.91 Debye). The dipole moment reflects the polarity of the molecule which increases with the increase in electronegativity of atoms. Also, it is related to the electronic distribution in a molecule and the chemical reactivity usually increases with the increase in the dipole moment as the interaction with other systems occurred. The recorded binding energy was 1059.84 eV.

The energy of the lowest occupied molecular orbital ( $E_{\text{HOMO}}$ ); the energy of the highest unoccupied molecular orbital ( $E_{\text{LUMO}}$ ) and energy gap,  $\Delta E$  (the gap between the HOMO and LUMO energy levels) and absolute hardness ( $\eta$ ) were calculated and represented in Fig 16. The absolute hardness;  $\eta$  ( $(E_{\text{LUMO}} - E_{\text{HOMO}})/2$ ) measures the molecular stability and reactivity. A hard molecular has a large energy gap while a soft molecule has a small energy gap [50]. The soft molecule is reactive and easily offers electrons to an acceptor. **14a** recorded  $\eta$  value of 1.4 eV as shown in Fig 16. In addition,  $\Delta E$  was found to be 2.835 eV smaller than those recorded for **9** and **13a**. This small  $\Delta E$  value of **14a** explains its reactivity side by side with proper hardness value which increases its tendency to be a good inhibitor towards VEGFR-2. As demonstrated in Fig 16, the electron density in HOMO is localized on 4-chlorophenyl acetamide moiety while in LUMO, the density is centered over the 5-(2-oxoindolin-3-ylidene)thiazolidine-2,4-dione moiety. The total density state confirmed the previous findings as the small energy gap of **14a** was noticed in the same value as presented in Fig 17. As the LUMO-HOMO energy gap decreases, the interactions between the reactants species, **13** and **9a** become stronger which results in a stable inhibitor structure.

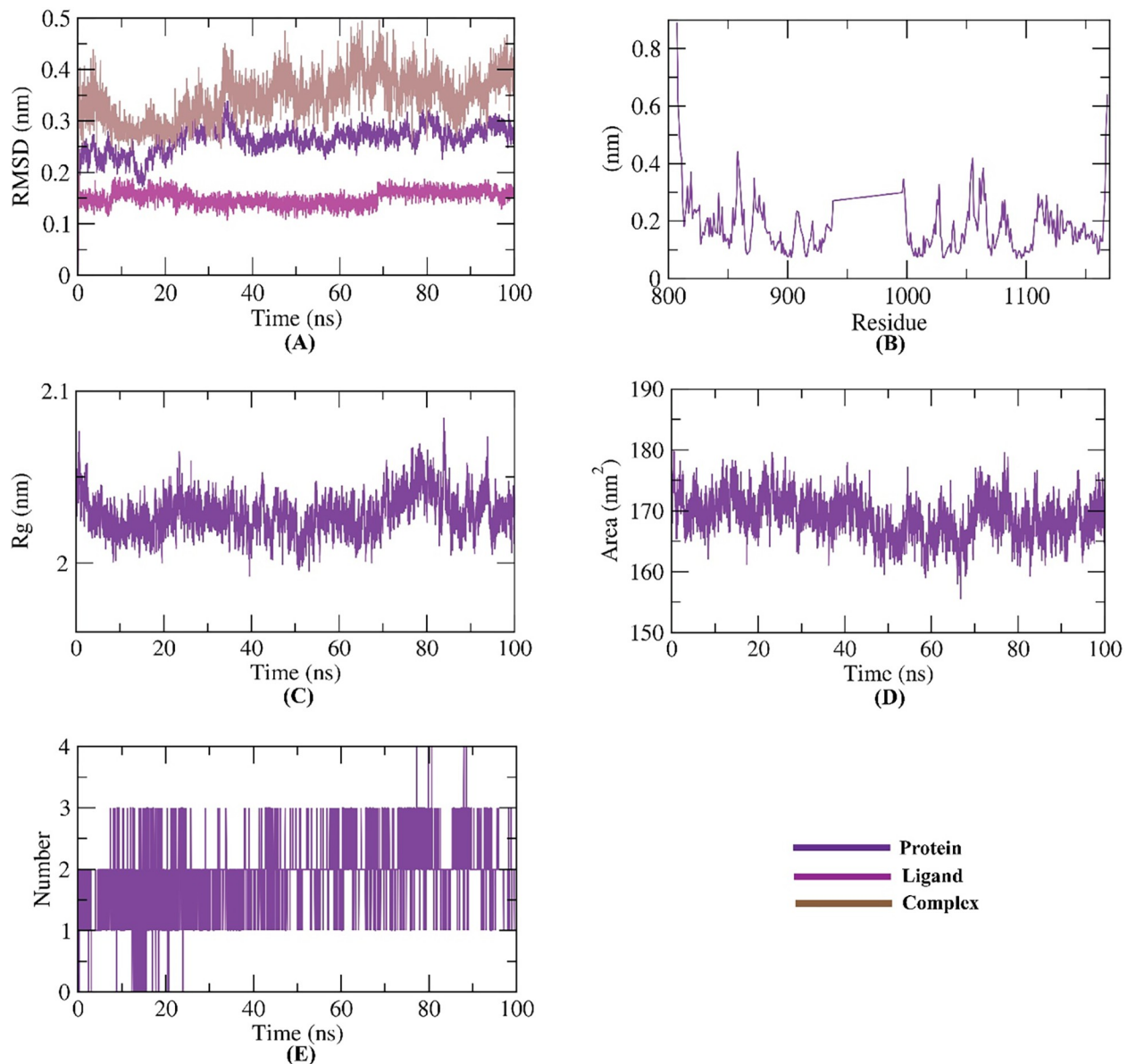


**Fig 11.** MD simulations experiments: A) RMSD values of **14a**-VEGFR-2 system before and after binding, B) RMSF of **14a**-VEGFR-2 system C)  $R_g$  of **14a**-VEGFR-2 system D) SASA of **14a**-VEGFR-2 system E) H-bonding between **14a**-VEGFR-2 system.

<https://doi.org/10.1371/journal.pone.0272362.g013>

Molecular electrostatic potential (MEP) illustrates the electronic charge distributions of molecules three dimensionally. MEP maps visualize variably charged zones of a molecule. Knowledge of the electron charge distributions can be used to explain how molecules interact with one another. The strength of the electrostatic potentials is well represented by the MEP surface in Fig 18. where red and blue regions mention the most electronegative electropositive zones, respectively. As shown in Fig 18, the oxygenated groups in all compounds have red color because these groups have negative electrostatic potential. For **14a**, oxygen atoms will behave as nucleophiles while blue regions at hydrogen atoms, mostly, behave as electrophiles [51].

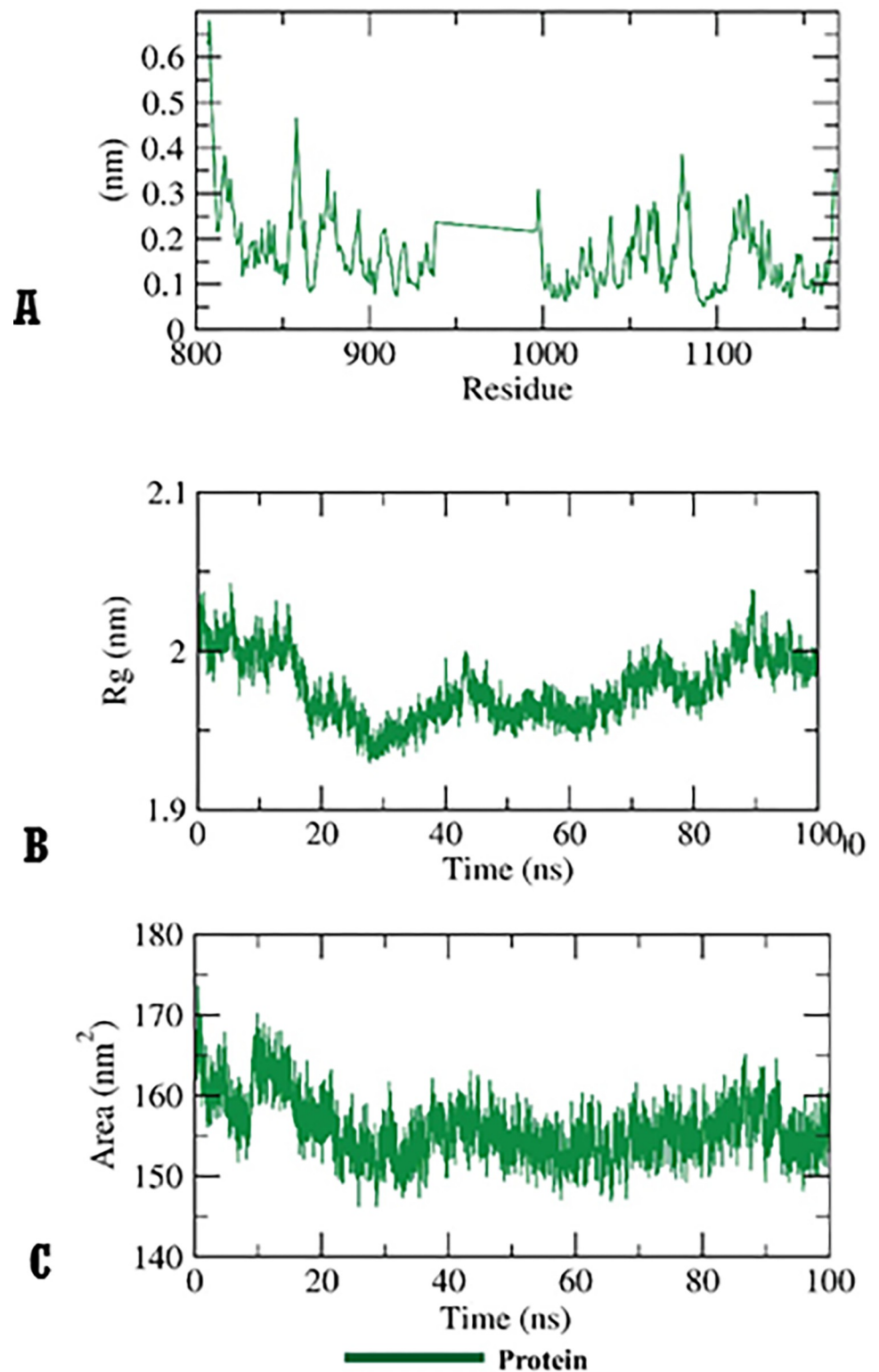
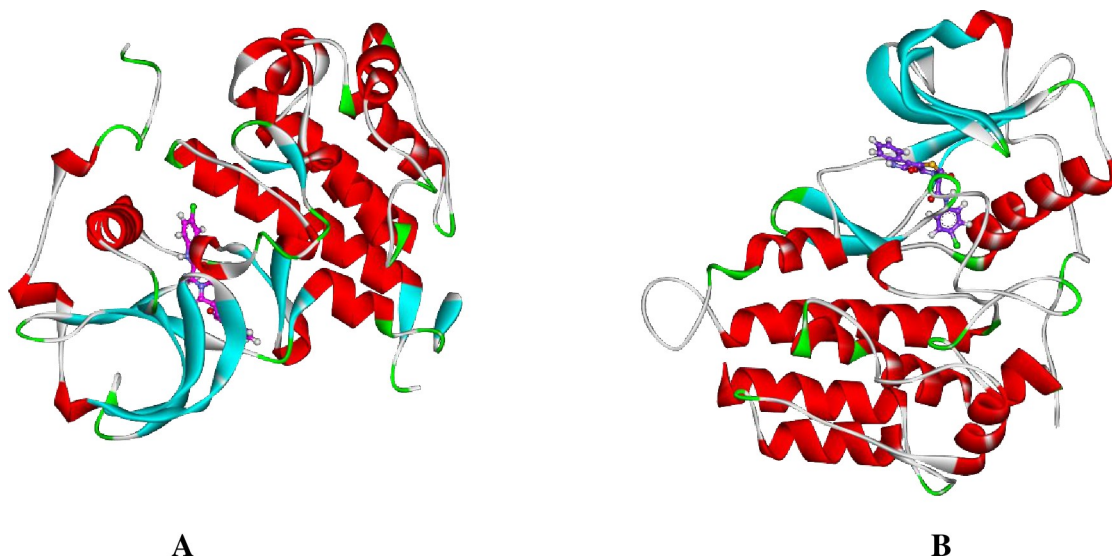


Fig 12. A) RMSF B)  $R_g$  C) SASA of VEGFR-2 enzyme in apo state.

<https://doi.org/10.1371/journal.pone.0272362.g014>



**Fig 13.** **14a**-VEGFR-2 structure at (A) 1 ns, (B) 100 ns.

<https://doi.org/10.1371/journal.pone.0272362.g015>

### 3. Conclusion

A new series of thiazolidine-2,4-diones derivatives were designed and synthesized as potential anticancer agents targeting VEGFR-2. These derivatives were tested for their anticancer efficacy against A549, Caco-2, HepG-2, and MDA-MB-231 cell lines. The most active antiproliferative member was found to be compound **14a** ( $IC_{50} = 1.5$  and  $31.5 \mu\text{M}$ ) against Caco-2 and HepG2 cell lines, respectively. In addition, when compared to the reference drug, sorafenib, kinase inhibition assay results revealed that all compounds had good inhibitory activity against VEGFR-2. Further, because of its high selectivity index, derivative **14a** was chosen for further testing of its effect on Caco-2 cell migration and alternation of Caco-2 cells gene expression. Compound **14a** significantly inhibited the ability of cancer cells to migrate and heal, according to a cell migration assay. Additionally, the ability of **14a** to downregulate Bcl-2, Survivin, and TGF expression levels was discovered in a subsequent biological assay. The ability of **14a** to recognize the ATP binding pocket of VEGFR-2 and elicit significant interactions with its key amino acids was demonstrated using molecular docking as well as several MD simulations studies. Also, the DFT calculations have been performed for **14a** inhibitor and free individual components, **13** and **9a** at B3LYB/6-311++G(d,p) level of theory. The results conducted that **14a** showed large stabilization due to the strong interaction forces within the molecule and small absolute hardness.

## 4. Experimental

### 4.1. Chemistry

**4.1.1. General.** The used chemical agents and devices in the synthesis procedures were described in **S.3 Section in S1 File**. Compounds **10a**, **b** and **14a-c** were furnished following the reported procedures [30, 31, 33, 34]. In **Table 7**, the colors, yields, and melting points of the new compounds were presented. The  $^1\text{H}$  NMR and  $^{13}\text{C}$  NMR analyses were carried out at 400 and 100 MHz, respectively in DMSO- $d_6$  as a solvent. the chemical shifts were presented as ppm. The infra-red analyses were carried out using KBr disc and the results were presented as  $\text{cm}^{-1}$ .

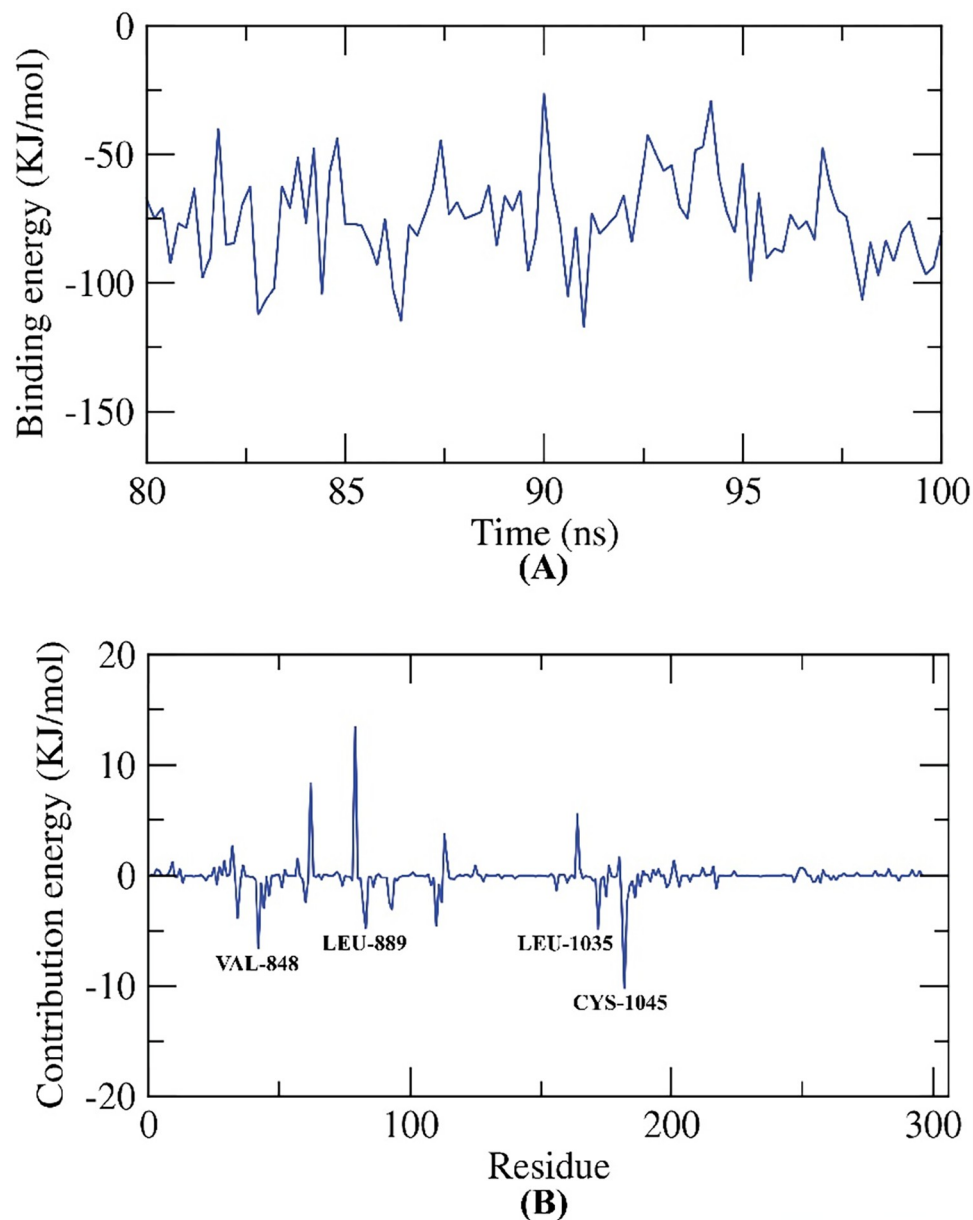
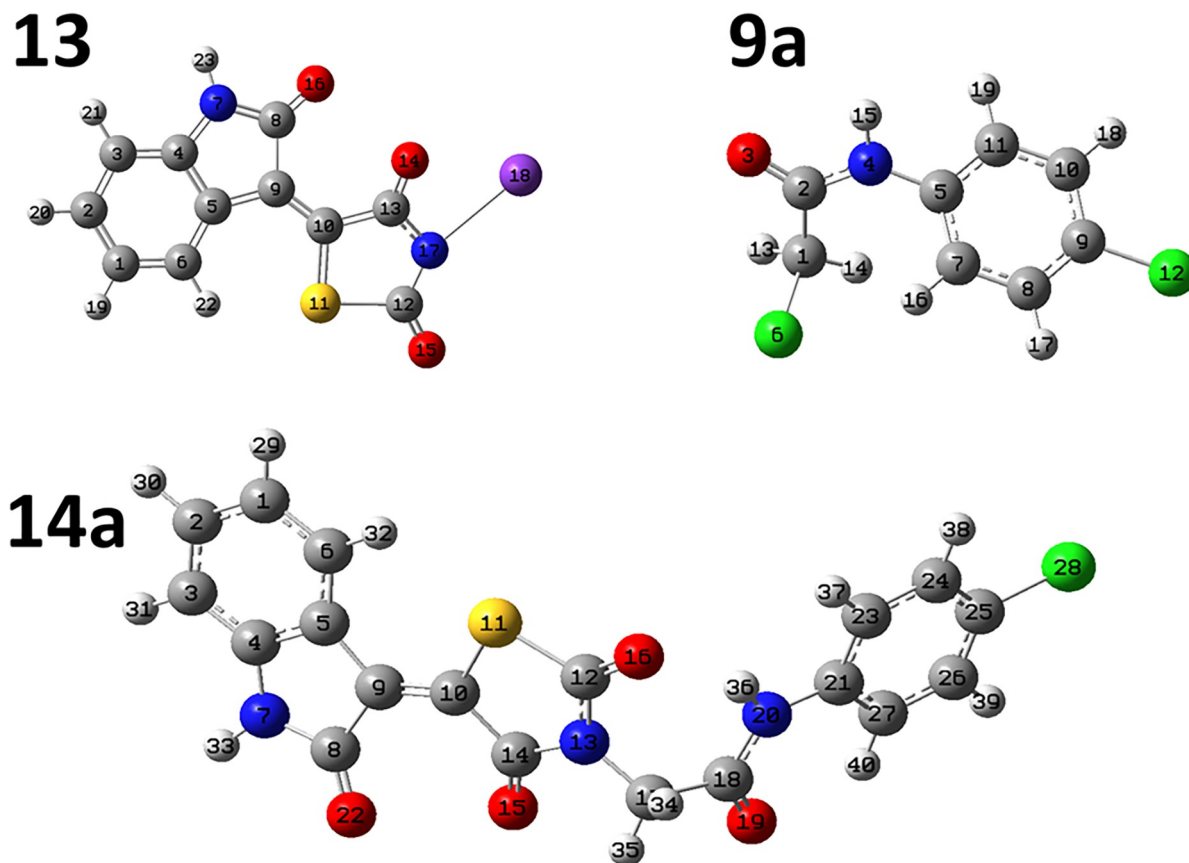


Fig 14. MM-PBSA experiments.

<https://doi.org/10.1371/journal.pone.0272362.g016>

**4.1.2. General synthesis pathway compounds 10a,b.** Compound 7 (0.001 mol) was heated with  $K_2CO_3$  in a dry DMF for 30 min. till formation of the corresponding *in situ* potassium salt 8. Then, the appropriate 2-chloro-*N*-substituted acetamide derivatives 9a, b (0.001 mol), and KI (0.001 mol) in DMF (10 ml) was added to the previous mixture with reflux on a water bath for 6 h. The reaction mixture was poured on crushed ice. The precipitate was filtered, dried, and crystallized from ethanol to give the corresponding target compounds 10a, b (Figs 19 & 20).

4.1.2.1. (*Z*)-*N*-(4-Chlorophenyl)-2-(5-((6-methoxy-2-oxo-1,2-dihydroquinolin-3-yl)methylene)-2,4-dioxothiazolidin-3-yl)acetamide (10a). IR: 3449, 3265 (NH), 3005 (CH aromatic)



**Fig 15.** The full optimized structure of 14a, 13 and 9a at B3LYB/6-311G++(d,p) basis set.

<https://doi.org/10.1371/journal.pone.0272362.g017>

2932 (CH aliphatic), 1724, 1673 (C = O);  $^1\text{H}$  NMR: 10.79 (s, 1H), 10.24 (s, 1H), 8.45 (s, 1H), 8.21 (s, 1H), 8.00 (d,  $J = 14.0$  Hz, 2H), 7.62 (d,  $J = 8.9$  Hz, 2H), 7.43 (m, 2H), 7.39 (d,  $J = 2.3$  Hz, 1H), 4.54 (s, 2H), 3.81 (s, 3H);  $^{13}\text{C}$  NMR: 171.63, 161.56, 160.73, 157.08, 155.01, 154.98, 142.25, 137.60, 136.51, 130.14, 130.08, 129.64, 127.02, 126.19, 124.16, 120.06, 119.61, 119.16, 117.30, 111.56, 56.03, 21.16.  $\text{C}_{22}\text{H}_{16}\text{ClN}_3\text{O}_5\text{S}$  (469.90).

4.1.2.2. (*Z*)-*N*-(2,5-Dichlorophenyl)-2-(5-((6-methoxy-2-oxo-1,2-dihydroquinolin-3-yl) methylene)-2,4-dioxothiazolidin-3-yl)acetamide (10b). IR: 3264 (NH), 3098 (CH aromatic) 2997, 2931 (CH aliphatic), 1753, 1688 (C = O);  $^1\text{H}$  NMR: 10.67 (s, 1H), 10.26 (s, 1H), 8.55 (s, 1H), 8.40 (s, 1H), 7.95 (d,  $J = 8$  Hz, 2H), 7.71 (m, 2H), 7.49 (d,  $J = 8.2$  Hz, 1H), 7.29–7.20 (m, 1H), 4.54 (s, 2H), 3.81 (s, 3H).  $\text{C}_{22}\text{H}_{15}\text{Cl}_2\text{N}_3\text{O}_5\text{S}$  (504.34).

**4.1.3. General synthesis pathway compounds 14a-c.** Compound 12 (0.001 mol) was heated with  $\text{K}_2\text{CO}_3$  in a dry DMF for 30 min. till formation of the corresponding *in situ* potassium salt 13. Then, the appropriate 2-chloro-*N*-substitutedacetamide derivatives 9a-c (0.001 mol), and KI (0.001 mol) in DMF (10 ml) was added to the previous mixture with reflux on a water bath for 6 h. The reaction mixture was poured on crushed ice. The precipitate was filtered, dried, and crystallized from ethanol to give the corresponding target compounds 14a-c (Figs 21–23).

4.1.3.1. *N*-(4-Chlorophenyl)-2-(2,4-dioxo-5-(2-oxoindolin-3-ylidene)thiazolidin-3-yl)acetamide (14a). IR: 3185, 3142 (NH), 3062 (CH aromatic), 1745, 1690 (C = O);  $^1\text{H}$  NMR: 11.32 (s, 1H), 10.58 (s, 1H), 8.78 (s, 1H), 7.60 (d,  $J = 8.5$  Hz, 2H), 7.48–7.37 (m, 3H), 7.09 (t,  $J = 7.8$  Hz,

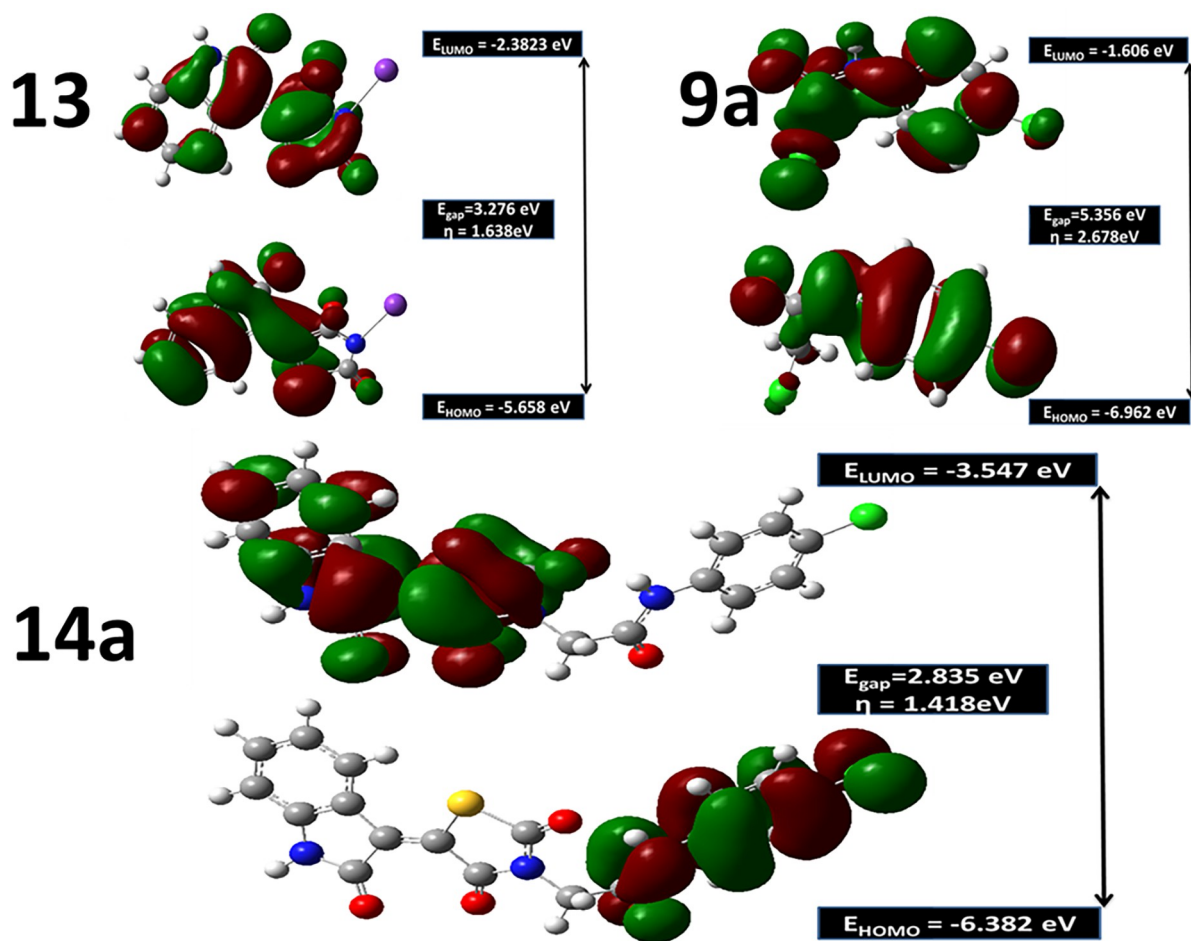


Fig 16. Frontier molecular orbitals, HOMO, LUMO, energy gaps,  $\Delta E$  and absolute hardness,  $\eta$  in eV for 14a inhibitor and free individual components, 13 and 9a at B3LYB/6-311++G(d,p) level.

<https://doi.org/10.1371/journal.pone.0272362.g018>

1H), 6.99 (d,  $J = 7.8$  Hz, 1H), 4.58 (s, 2H);  $^{13}\text{C}$  NMR: 170.23, 168.72, 165.68, 164.47, 144.64 (2C), 137.78, 133.59, 129.31 (2C), 128.43, 128.25, 127.83, 122.68, 121.28 (2C), 120.22, 111.17, 44.13.  $\text{C}_{19}\text{H}_{12}\text{ClN}_3\text{O}_4\text{S}$  (413.83).

4.1.3.2. *N*-(2,5-Dichlorophenyl)-2-(2,4-dioxo-5-(2-oxoindolin-3-ylidene)thiazolidin-3-yl)acetamide (14b). IR: 3211, 3176 (NH), 3065 (CH aromatic) 2994, 2949 (CH aliphatic), 1744, 1696 (C = O);  $^1\text{H}$  NMR: 11.32 (s, 1H), 10.24 (s, 1H), 8.78 (d,  $J = 7.9$  Hz, 1H), 7.88 (d,  $J = 2.5$  Hz, 1H), 7.58 (d,  $J = 8.7$  Hz, 1H), 7.44 (t,  $J = 7.7$  Hz, 1H), 7.31 (dd,  $J = 8.6, 2.6$  Hz, 1H), 7.12 (d,  $J = 7.8$  Hz, 1H), 6.99 (d,  $J = 7.8$  Hz, 1H), 4.70 (s, 2H);  $^{13}\text{C}$  NMR: 170.26, 168.72, 165.70, 163.97, 144.60, 136.31, 133.56, 133.24, 129.74 (2C), 129.40, 128.42, 128.17, 122.67, 120.21, 119.71 (2C), 111.15, 44.06.  $\text{C}_{19}\text{H}_{11}\text{Cl}_2\text{N}_3\text{O}_4\text{S}$  (448.27).

4.1.3.3. 2-(2,4-Dioxo-5-(2-oxoindolin-3-ylidene)thiazolidin-3-yl)-*N*-phenethylacetamide (14c). IR: 3303, 3179 (NH), 3062 (CH aromatic) 2935, 2886 (CH aliphatic), 1744, 1691 (C = O);  $^1\text{H}$  NMR: 11.31 (s, 1H), 8.82 (dd,  $J = 18.2, 7.0$  Hz, 2H), 7.45 (t,  $J = 7.7$  Hz, 1H), 7.35 (t,  $J = 7.5$  Hz, 2H), 7.28 (d,  $J = 7.7$  Hz, 3H), 7.12 (t,  $J = 7.8$  Hz, 1H), 6.99 (d,  $J = 7.8$  Hz, 1H), 4.40 (s, 2H), 4.34 (t, 2H), 3.40 (t, 2H);  $^{13}\text{C}$  NMR: 170.30, 168.74, 165.75, 165.61, 144.54, 139.31, 133.48, 129.88, 128.82 (2C), 128.39, 127.89, 127.66 (2C), 127.42, 122.67, 120.24, 111.14, 43.66, 42.75, 31.18.  $\text{C}_{21}\text{H}_{17}\text{N}_3\text{O}_4\text{S}$  (407.44).

## 4.2. Biological testing

**4.2.1. *In vitro* anti-proliferative activity.** The synthesized compounds were evaluated for their anti-proliferative activities against A549, Caco-2, HepG2, and MDA-mb-231 cell lines using the MTT assay protocol [52–54] as described in **S.1.2. Section in S1 File**.

**4.2.2. *In vitro* VEGFR-2 inhibition.** VEGFR-2 ELISA kit was used in this test as described in **S.1.3. Section in S1 File** [24, 55, 56].

**4.2.3. Safety assay.** The safety profiles of the tested compounds were checked on one non-cancerous cell line (Vero) to determine the treatments concentrations that do not depict toxic effects against the tested cells as described in **S.1.1. Section in S1 File** [57].

**4.2.4. Selectivity index (SI).** The selectivity index values of the tested compounds on cancer cells were calculated as described (**S.1.4 Section in S1 File**) [58].

**4.2.5. Cell Migration assay.** Cell Migration assay was conducted according to the reported protocol as described [59] in **S.1.5. Section in S1 File**.

**4.2.6. Gene expression pattern.** The molecular anticancer mode of action of **14a** was investigated by screening their ability to control the gene expression levels of Bcl2, Bcl-xl, TGF and Survivin genes as reported [60] in **S.1.6. Section in S1 File**.

## 4.3. *In silico* studies

**4.3.1. Docking studies.** MOE2019 software was used to perform docking studies against VEGFR-2 [PDB ID: 4ASD] [61–65] as described in **S.2.1. Section in S1 File**.

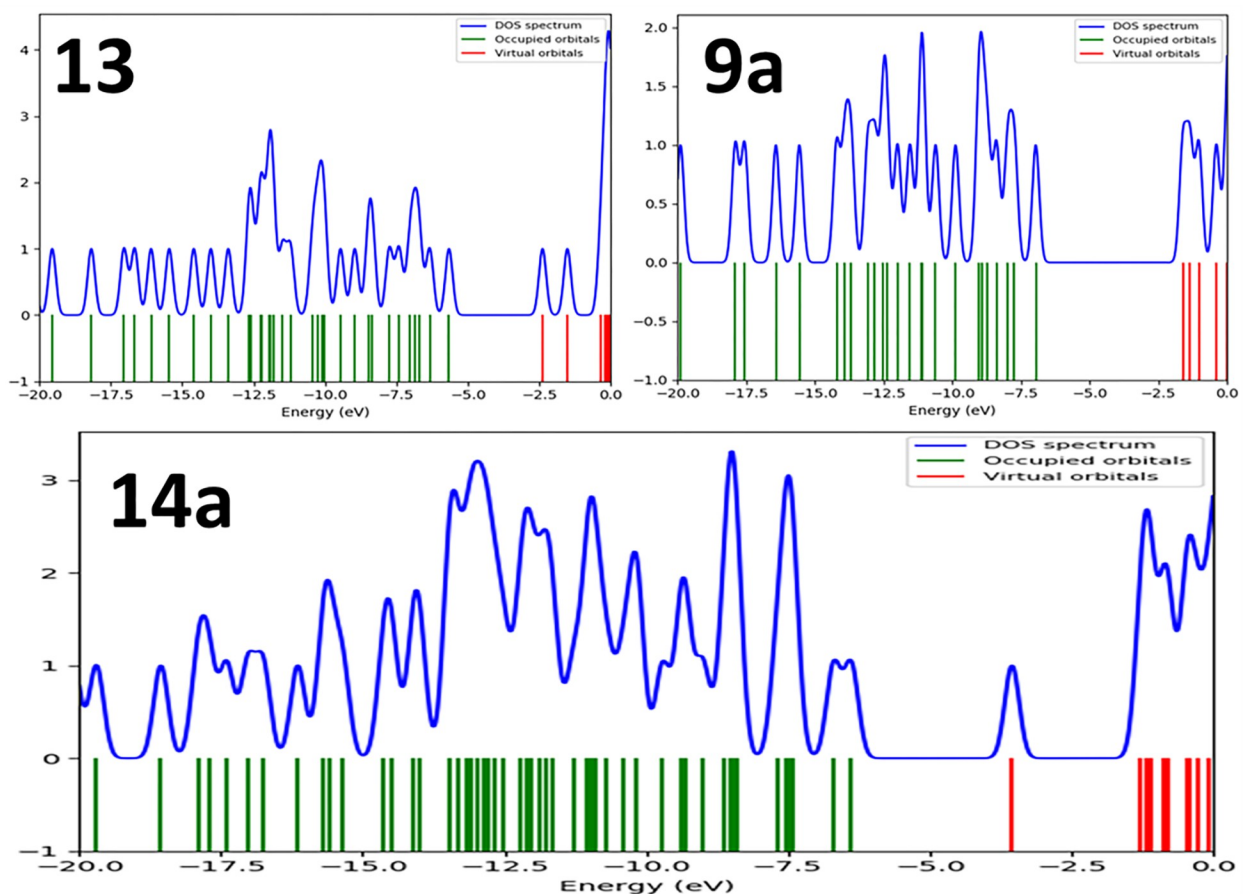


**Fig 17.** Total density of state, TDOS for **14a** inhibitor and free individual components, **13** and **9a** at B3LYB/6-311++G(d,p) level.

<https://doi.org/10.1371/journal.pone.0272362.g019>

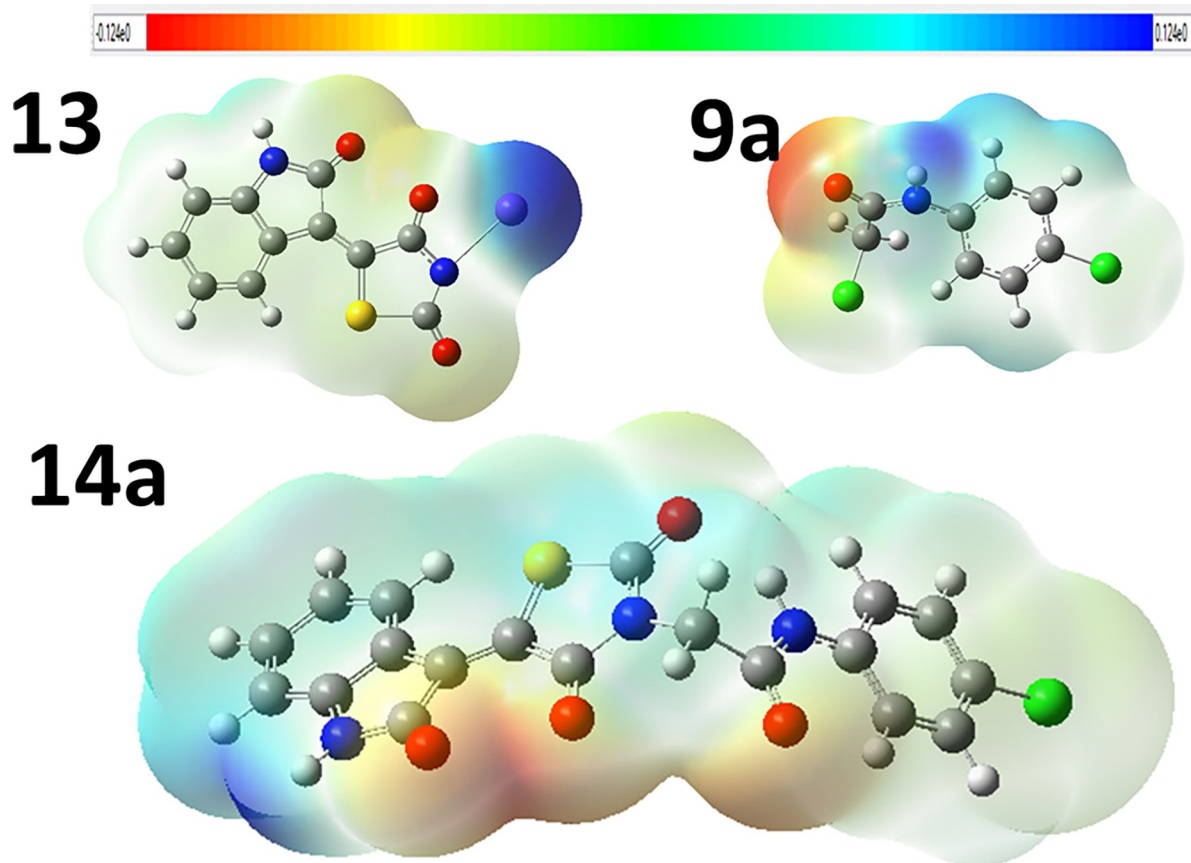


**Fig 18.** Molecular electrostatic potentials for 14a inhibitor and free individual components, 13 and 9a at B3LYB/6-311++G(d,p) level of theory.

<https://doi.org/10.1371/journal.pone.0272362.g020>

**4.3.2. ADMET studies.** Discovery studio 4.0 was used to perform ADMET studies as reported in before [43, 65–69] (S.2.2. Section in S1 File).

**4.3.3. Toxicity studies.** Discovery studio 4.0 was used to carry out the toxicity studies as described [18, 70–72] in S.2.3. Section in S1 File.

**4.3.4. Molecular dynamics simulation & MM/PBSA.** MD simulation experiments and MM/PBSA (Molecular Mechanics/Poisson Boltzmann Surface Area) were carried out using GROMACS as reported in S.2.4 & S.2.5. Sections in S1 File [67, 73–75].

**4.4.4. Density Function Theory (DFT) calculations.** The DFT calculations were performed using Gaussian 09 software and the output files were visualized using GaussianView5.

**Table 7.** The colors, yields, and melting points of the new compounds.

| Compounds | Color          | Yield | Meting points (°C) |
|-----------|----------------|-------|--------------------|
| 10a       | White powder   | 74%   | 265–267            |
| 10b       | Yellow powder  | 70%   | 234–236            |
| 14a       | White crystals | 76%   | 224–226            |
| 14b       | Yellow powder  | 78%   | 230–232            |
| 14c       | White powder   | 80%   | 250–252            |

<https://doi.org/10.1371/journal.pone.0272362.t007>

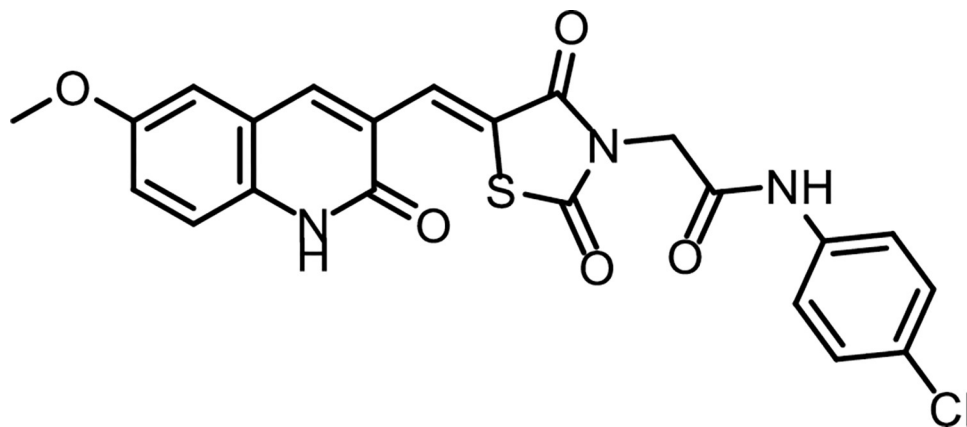


Fig 19. Chemical structure of compound 10a.

<https://doi.org/10.1371/journal.pone.0272362.g021>

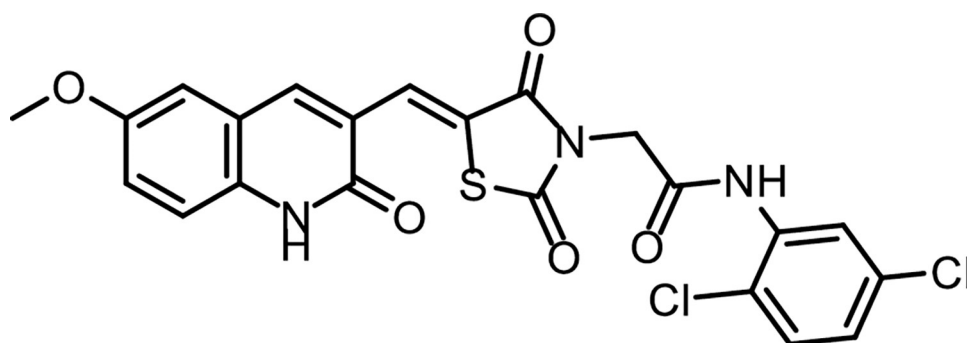


Fig 20. Chemical structure of compound 10b.

<https://doi.org/10.1371/journal.pone.0272362.g022>

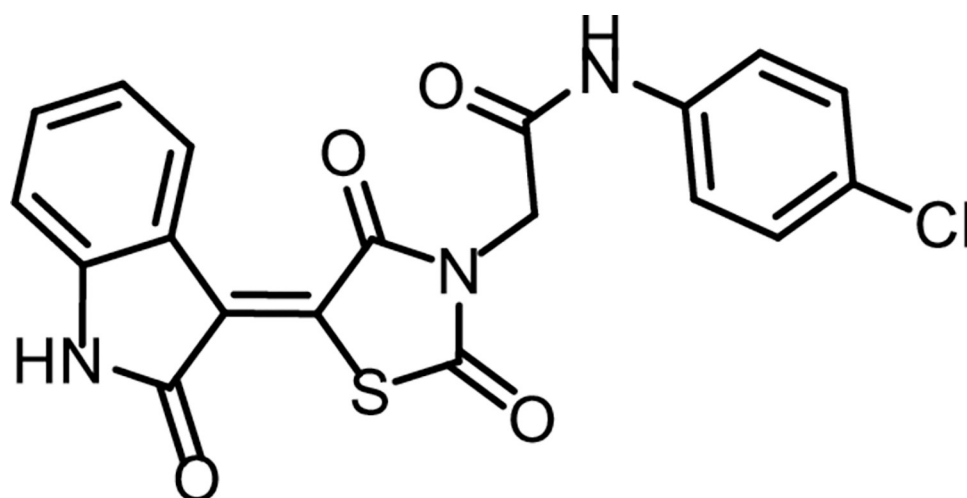


Fig 21. Chemical structure of compound 14a.

<https://doi.org/10.1371/journal.pone.0272362.g023>

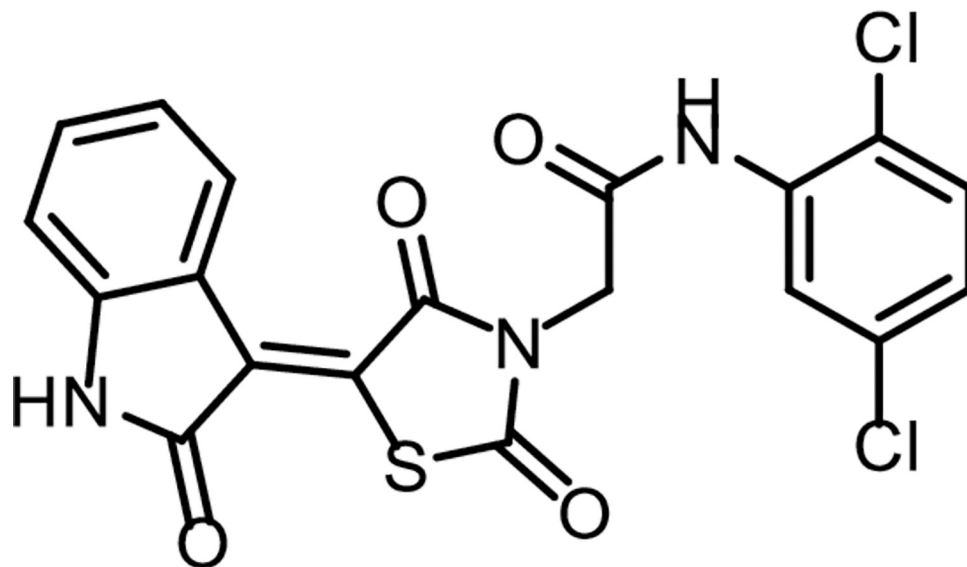


Fig 22. Chemical structure of compound 14b.

<https://doi.org/10.1371/journal.pone.0272362.g024>

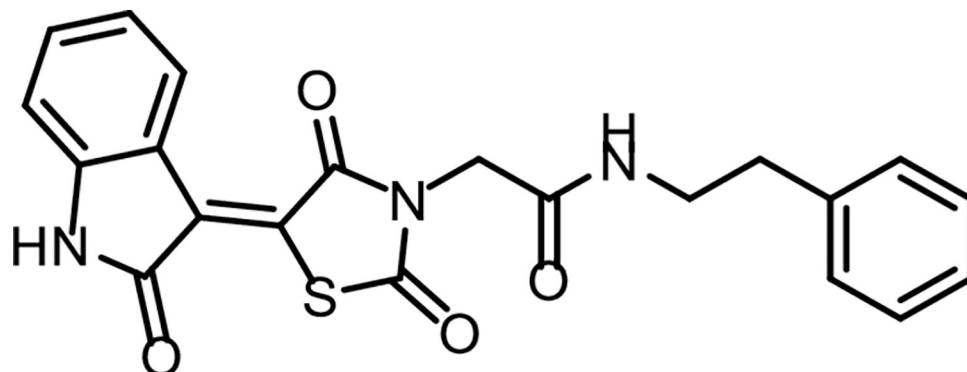


Fig 23. Chemical structure of compound 14c.

<https://doi.org/10.1371/journal.pone.0272362.g025>

Total density of state (TDOS) was calculated and analyzed using GaussSum software. Chem3D 15 was used to draw the original chemical structures of all compounds. The DFT (B3LYP) method with 6-311G++(d,p) basis set to optimize organic structure compounds.

## Supporting information

**S1 File.** Supporting information related to this manuscript is found in a separate file. (PDF)

## Author Contributions

**Conceptualization:** Ibrahim H. Eissa.

**Data curation:** Nehal El-Deeb, Ahmed M. Kenawy.

**Formal analysis:** Nehal El-Deeb, Ahmed M. Kenawy, Mohamed S. Alesawy.

**Funding acquisition:** Eslam B. Elkaeed, Bshra A. Alsouk.

**Investigation:** Wagdy M. Eldehna, Mohamed S. Alesawy, Ibrahim H. Eissa.

**Methodology:** Mohammed S. Taghour, Nehal El-Deeb, Ahmed M. Kenawy, Dalal Z. Husein.

**Project administration:** Ahmed M. Metwaly, Ibrahim H. Eissa.

**Resources:** Wagdy M. Eldehna.

**Software:** Hazem Elkady.

**Supervision:** Ahmed M. Metwaly, Ibrahim H. Eissa.

**Validation:** Dalal Z. Husein, Ahmed M. Metwaly.

**Writing – original draft:** Hazem Elkady, Mohamed S. Alesawy.

**Writing – review & editing:** Wagdy M. Eldehna, Ahmed M. Kenawy, Eslam B. Elkaeed, Bshra A. Alsouk, Ahmed M. Metwaly, Ibrahim H. Eissa.

## References

1. El-Dash Y., Elzayat E., Abdou A.M., Hassan R.A., Novel thienopyrimidine-aminothiazole hybrids: design, synthesis, antimicrobial screening, anticancer activity, effects on cell cycle profile, caspase-3 mediated apoptosis and VEGFR-2 inhibition, *Bioorganic Chemistry* 114 (2021) 105137. <https://doi.org/10.1016/j.bioorg.2021.105137> PMID: 34237644
2. Mahdy H.A., Ibrahim M.K., Metwaly A.M., Belal A., Mehany A.B., El-Gamal K.M., et al, Design, synthesis, molecular modeling, in vivo studies and anticancer evaluation of quinazolin-4 (3H)-one derivatives as potential VEGFR-2 inhibitors and apoptosis inducers, *Bioorganic Chemistry* 94 (2020) 103422. <https://doi.org/10.1016/j.bioorg.2019.103422> PMID: 31812261
3. El-Adl K., El-Helby A.-G.A., Sakr H., Eissa I.H., El-Hddad S.S., Shoman F.M., Design, synthesis, molecular docking and anticancer evaluations of 5-benzylidenethiazolidine-2, 4-dione derivatives targeting VEGFR-2 enzyme, *Bioorganic Chemistry* (2020) 104059. <https://doi.org/10.1016/j.bioorg.2020.104059> PMID: 32653608
4. Olsson A.-K., Dimberg A., Kreuger J., Claesson-Welsh L., VEGF receptor signalling? In control of vascular function, *Nature reviews Molecular cell biology* 7(5) (2006) 359–371. <https://doi.org/10.1038/nrm1911> PMID: 16633338
5. Niu G., Chen X., Vascular endothelial growth factor as an anti-angiogenic target for cancer therapy, *Current drug targets* 11(8) (2010) 1000–1017. <https://doi.org/10.2174/138945010791591395> PMID: 20426765
6. Shibuya M., Vascular endothelial growth factor (VEGF) and its receptor (VEGFR) signaling in angiogenesis: a crucial target for anti- and pro-angiogenic therapies, *Genes & cancer* 2(12) (2011) 1097–1105.
7. Elrazaz E.Z., Serya R.A., Ismail N.S., Albohy A., Abou El Ella D.A., Abouzid K.A., Discovery of Potent Thieno [2, 3-d] pyrimidine VEGFR-2 Inhibitors: Design, Synthesis and Enzyme Inhibitory Evaluation Supported by Molecular Dynamics Simulations, *Bioorganic Chemistry* (2021) 105019. <https://doi.org/10.1016/j.bioorg.2021.105019> PMID: 34091286
8. Lee K., Jeong K.-W., Lee Y., Song J.Y., Kim M.S., Lee G.S., et al, Pharmacophore modeling and virtual screening studies for new VEGFR-2 kinase inhibitors, *European journal of medicinal chemistry* 45(11) (2010) 5420–5427. <https://doi.org/10.1016/j.ejmech.2010.09.002> PMID: 20869793
9. Machado V.A., Peixoto D., Costa R., Froufe H.J., Calhelha R.C., Abreu R.M., et al, Synthesis, antiangiogenesis evaluation and molecular docking studies of 1-aryl-3-[(thieno [3, 2-b] pyridin-7-ylthio) phenyl] ureas: Discovery of a new substitution pattern for type II VEGFR-2 Tyr kinase inhibitors, *Biorg. Med. Chem.* 23(19) (2015) 6497–6509. <https://doi.org/10.1016/j.bmc.2015.08.010> PMID: 26344591
10. Garofalo A., Goossens L., Six P., Lemoine A., Ravez S., Farce A., et al, Impact of aryloxy-linked quinazolinones: A novel series of selective VEGFR-2 receptor tyrosine kinase inhibitors, *Bioorg. Med. Chem. Lett.* 21(7) (2011) 2106–2112. <https://doi.org/10.1016/j.bmcl.2011.01.137> PMID: 21353546
11. Marrone T.J., Briggs a., James M J.A. McCammon, Structure-based drug design: computational advances, *Annual review of pharmacology and toxicology* 37(1) (1997) 71–90.
12. Li N., Wang Y., Li W., Li H., Yang L., Wang J., et al, Screening of Some Sulfonamide and Sulfonamide Derivatives as Anti-Alzheimer's Agents Targeting BACE1 and PPARY, *Journal of Chemistry* 2020 (2020).

13. Abdel-Aziz H.A., Eldehna W.M., Fares M., Al-Rashood S.T., Al-Rashood K.A., Abdel-Aziz M.M., et al, Synthesis, biological evaluation and 2D-QSAR study of halophenyl bis-hydrazones as antimicrobial and antitubercular agents, *International journal of molecular sciences* 16(4) (2015) 8719–8743. <https://doi.org/10.3390/ijms16048719> PMID: 25903147
14. Akram M., Lal H., Shakya S., Varshney R., Molecular engineering of complexation between RNA and biodegradable cationic gemini surfactants: role of the hydrophobic chain length, *Molecular Systems Design & Engineering* (2022).
15. Hasan A.H., Murugesan S., Amran S.I., Chander S., Alanazi M.M., Hadda T.B., et al, Novel thiophene Chalcones-Coumarin as acetylcholinesterase inhibitors: Design, synthesis, biological evaluation, molecular docking, ADMET prediction and molecular dynamics simulation, *Bioorganic Chemistry* 119 (2022) 105572. <https://doi.org/10.1016/j.bioorg.2021.105572> PMID: 34971946
16. Alhomrani M., Alsanie W.F., Alamri A.S., Alyami H., Habeeballah H., Alkhatabi H.A., et al, Enhancing the Antipsychotic Effect of Risperidone by Increasing Its Binding Affinity to Serotonin Receptor via Picric Acid: A Molecular Dynamics Simulation, *Pharmaceuticals* 15(3) (2022) 285. <https://doi.org/10.3390/ph15030285> PMID: 35337083
17. Abbass E.M., Khalil A.K., Mohamed M.M., Eissa I.H., A.M.J.B.c. El-Naggar, Design, efficient synthesis, docking studies, and anticancer evaluation of new quinoxalines as potential intercalative Topo II inhibitors and apoptosis inducers, 104 (2020) 104255.
18. El-Adl K., Ibrahim M.-K., Alesawy M.S., Eissa I.H.J.B., Chemistry M., [1, 2, 4] Triazolo [4, 3-c] quinazoline and bis ([1, 2, 4] triazolo)[4, 3-a: 4', 3'-c] quinazoline derived DNA intercalators: Design, synthesis, in silico ADMET profile, molecular docking and anti-proliferative evaluation studies, 30 (2021) 115958. <https://doi.org/10.1016/j.bmc.2020.115958> PMID: 33360576
19. Hagra M., El Deeb M.A., Elzahabi H.S., Elkaeed E.B., Mehany A.B., Eissa I.H.J.J.o.e.i., m. chemistry, Discovery of new quinolines as potent colchicine binding site inhibitors: design, synthesis, docking studies, and anti-proliferative evaluation, 36(1) (2021) 640–658.
20. Eissa I.H., Dahab M.A., Ibrahim M.K., Alsaif N.A., Alanazi A., Eissa S.I., et al, Design and discovery of new antiproliferative 1, 2, 4-triazin-3 (2H)-ones as tubulin polymerization inhibitors targeting colchicine binding site, 112 (2021) 104965. <https://doi.org/10.1016/j.bioorg.2021.104965> PMID: 34020238
21. El-Metwally S.A., Abou-El-Regal M.M., Eissa I.H., Mehany A.B., Mahdy H.A., Elkady H., et al, Discovery of thieno [2, 3-d] pyrimidine-based derivatives as potent VEGFR-2 kinase inhibitors and anti-cancer agents, 112 (2021) 104947. <https://doi.org/10.1016/j.bioorg.2021.104947> PMID: 33964580
22. El-Adl K., Sakr H.M., Yousef R.G., Mehany A.B., Metwaly A.M., Elhendawy M.A., et al, Discovery of new quinoxaline-2 (1H)-one-based anticancer agents targeting VEGFR-2 as inhibitors: Design, synthesis, and anti-proliferative evaluation, 114 (2021) 105105. <https://doi.org/10.1016/j.bioorg.2021.105105> PMID: 34175720
23. Parmar D.R., Soni J.Y., Guduru R., Rayani R.H., Kusurkar R.V., Vala A.G., et al, Discovery of new anti-cancer thiourea-azetidine hybrids: Design, synthesis, in vitro antiproliferative, SAR, in silico molecular docking against VEGFR-2, ADMET, toxicity, and DFT studies, 115 (2021) 105206.
24. Alanazi M.M., Eissa I.H., Alsaif N.A., Obaidullah A.J., Alanazi W.A., Alasmari A.F., et al, Design, synthesis, docking, ADMET studies, and anticancer evaluation of new 3-methylquinoxaline derivatives as VEGFR-2 inhibitors and apoptosis inducers, *Journal of Enzyme Inhibition and Medicinal Chemistry*, 36 (1) (2021) 1760–1782. <https://doi.org/10.1080/14756366.2021.1956488> PMID: 34340610
25. Yousef R.G., Sakr H.M., Eissa I.H., Mehany A.B., Metwaly A.M., Elhendawy M.A., et al, New quinoxaline-2 (1 H)-ones as potential VEGFR-2 inhibitors: design, synthesis, molecular docking, ADMET profile and anti-proliferative evaluations, 45(36) (2021) 16949–16964.
26. Alanazi M.M., Elwan A., Alsaif N.A., Obaidullah A.J., Alkahtani H.M., Al-Mehizia A.A., et al M. Chemistry, Discovery of new 3-methylquinoxalines as potential anti-cancer agents and apoptosis inducers targeting VEGFR-2: Design, synthesis, and in silico studies, 36(1) (2021) 1732–1750.
27. Ran F., Li W., Qin Y., Yu T., Liu Z., Zhou M., et al, c. longevity, Inhibition of vascular smooth muscle and cancer cell proliferation by new VEGFR inhibitors and their immunomodulator effect: design, synthesis, and biological evaluation, 2021 (2021).
28. Elkady H., Elwan A., El-Mahdy H.A., Doghish A.S., Ismail A., Taghour M.S., et al, m. chemistry, New benzoxazole derivatives as potential VEGFR-2 inhibitors and apoptosis inducers: design, synthesis, anti-proliferative evaluation, flowcytometric analysis, and in silico studies, 37(1) (2022) 397–410.
29. Meth-Cohn O., Narine B., Tarnowski B., A versatile new synthesis of quinolines and related fused pyridines. Part II, *Tetrahedron Letters* 20(33) (1979) 3111–3114.
30. Kar K., Krithika U., Basu P., Kumar S.S., Reji A., Kumar B.P., Design, synthesis and glucose uptake activity of some novel glitazones, *Bioorganic chemistry* 56 (2014) 27–33. <https://doi.org/10.1016/j.bioorg.2014.05.006> PMID: 24927033

31. Abdel-Wahab B.F., Khidre R.E., 2-Chloroquinoline-3-carbaldehyde II: synthesis, reactions, and applications, *Journal of Chemistry* 2013 (2013).
32. Yu Y.-C., Kuang W.-B., Huang R.-Z., Fang Y.-L., Zhang Y., Chen Z.-F., et al, Design, synthesis and pharmacological evaluation of new 2-oxo-quinoline derivatives containing  $\alpha$ -aminophosphonates as potential antitumor agents, *MedChemComm* 8(6) (2017) 1158–1172. <https://doi.org/10.1039/c7md00098g> PMID: 30108826
33. Bruno G., Costantino L., Curinga C., Maccari R., Monforte F., Nicolo F., et al, Synthesis and aldose reductase inhibitory activity of 5-arylidene-2, 4-thiazolidinediones, *Bioorganic & medicinal chemistry* 10 (4) (2002) 1077–1084. [https://doi.org/10.1016/s0968-0896\(01\)00366-2](https://doi.org/10.1016/s0968-0896(01)00366-2) PMID: 11836118
34. Evdokimov N.M., Magedov I.V., McBrayer D., Kornienko A., Isatin derivatives with activity against apoptosis-resistant cancer cells, *Bioorganic & medicinal chemistry letters* 26(6) (2016) 1558–1560. <https://doi.org/10.1016/j.bmcl.2016.02.015> PMID: 26883150
35. Datar P.A., Aher S.B., Design and synthesis of novel thiazolidine-2, 4-diones as hypoglycemic agents, *Journal of Saudi Chemical Society* 20 (2016) S196–S201.
36. Pritchett J.C., Naesens L., Montoya J., Treating HHV-6 infections: The laboratory efficacy and clinical use of anti-HHV-6 agents, (2014).
37. Peña-Morán O.A., Villarreal M.L., Álvarez-Berber L., Meneses-Acosta A., Rodríguez-López V.J.M., Cytotoxicity, post-treatment recovery, and selectivity analysis of naturally occurring podophyllotoxins from *Bursera fagaroides* var. *fagaroides* on breast cancer cell lines, 21(8) (2016) 1013.
38. Liang C.-C., Park A.Y., Guan J.-L., In vitro scratch assay: a convenient and inexpensive method for analysis of cell migration in vitro, *Nature protocols* 2(2) (2007) 329–333. <https://doi.org/10.1038/nprot.2007.30> PMID: 17406593
39. Yang J., Song K., Krebs T.L., Jackson M.W., Danielpour D., Rb/E2F4 and Smad2/3 link survivin to TGF- $\beta$ -induced apoptosis and tumor progression, *Oncogene* 27(40) (2008) 5326–5338.
40. Kim R., Unknotting the roles of Bcl-2 and Bcl-xL in cell death, *Biochemical and biophysical research communications* 333(2) (2005) 336–343. <https://doi.org/10.1016/j.bbrc.2005.04.161> PMID: 15922292
41. El-Helby A.-G.A., Ayyad R.R., El-Adl K., Elkady H., Phthalazine-1, 4-dione derivatives as non-competitive AMPA receptor antagonists: design, synthesis, anticonvulsant evaluation, ADMET profile and molecular docking, *Molecular diversity* 23(2) (2019) 283–298. <https://doi.org/10.1007/s11030-018-9871-y> PMID: 30168051
42. El-Helby A.G.A., Ayyad R.R., Zayed M.F., Abulkhair H.S., Elkady H., El-Adl K., Design, synthesis, in silico ADMET profile and GABA-A docking of novel phthalazines as potent anticonvulsants, *Archiv Der Pharmazie* 352(5) (2019) 1800387. <https://doi.org/10.1002/ardp.201800387> PMID: 30989729
43. Abdallah A.E., Alesawy M.S., Eissa S.I., El-Fakharany E.M., Kalaba M.H., Sharaf M.H., et al, Design and synthesis of new 4-(2-nitrophenoxy) benzamide derivatives as potential antiviral agents: Molecular modeling and in vitro antiviral screening, *New Journal of Chemistry* 45(36) (2021) 16557–16571.
44. Xia X., Maliski E.G., Gallant P., Rogers D., Classification of kinase inhibitors using a Bayesian model, *Journal of medicinal chemistry* 47(18) (2004) 4463–4470. <https://doi.org/10.1021/jm0303195> PMID: 15317458
45. BIOVIA, QSAR, ADMET and Predictive Toxicology. <https://www.3dsbiovia.com/products/collaborative-science/biovia-discovery-studio/qsar-admet-and-predictive-toxicology.html>. (Accessed May 2020).
46. Sousa S.F., Fernandes P.A., Ramos M.J., Protein–ligand docking: current status and future challenges, *Proteins: Structure, Function, and Bioinformatics* 65(1) (2006) 15–26.
47. Hollingsworth S.A., Dror R.O., Molecular dynamics simulation for all, *Neuron* 99(6) (2018) 1129–1143. <https://doi.org/10.1016/j.neuron.2018.08.011> PMID: 30236283
48. Hansson T., Oostenbrink C., van Gunsteren W., Molecular dynamics simulations, *Current opinion in structural biology* 12(2) (2002) 190–196. [https://doi.org/10.1016/s0959-440x\(02\)00308-1](https://doi.org/10.1016/s0959-440x(02)00308-1) PMID: 11959496
49. Durrant J.D., McCammon J.A., Molecular dynamics simulations and drug discovery, *BMC biology* 9(1) (2011) 1–9. <https://doi.org/10.1186/1741-7007-9-71> PMID: 22035460
50. Wang T., Husein D.Z., Novel synthesis of multicomponent porous nano-hybrid composite, theoretical investigation using DFT and dye adsorption applications: disposing of waste with waste, *Environmental Science and Pollution Research* (2022) 1–28.
51. Husein D.Z., Hassanien R., Khamis M., Cadmium oxide nanoparticles/graphene composite: synthesis, theoretical insights into reactivity and adsorption study, *RSC Advances* 11(43) (2021) 27027–27041. <https://doi.org/10.1039/d1ra04754j> PMID: 35480026
52. Thabrew M.I., Hughes R.D., McFarlane I.G., Screening of hepatoprotective plant components using a HepG2 cell cytotoxicity assay, *Journal of pharmacy and pharmacology* 49(11) (1997) 1132–1135. <https://doi.org/10.1111/j.2042-7158.1997.tb06055.x> PMID: 9401951

53. El-Deeb N.M., Ibrahim O.M., Mohamed M.A., Farag M.M., Farrag A.A., El-Aassar M., Alginate/k-carrageenan oral microcapsules loaded with *Agaricus bisporus* polysaccharides MH751906 for natural killer cells mediated colon cancer immunotherapy, *International Journal of Biological Macromolecules* (2022). <https://doi.org/10.1016/j.ijbiomac.2022.02.058> PMID: 35183600
54. El-Zahabi M.A., Sakr H., El-Adl K., Zayed M., Abdelraheem A.S., Eissa S.I., et al, Design, synthesis, and biological evaluation of new challenging thalidomide analogs as potential anticancer immunomodulatory agents, *Bioorganic chemistry* 104 (2020) 104218. <https://doi.org/10.1016/j.bioorg.2020.104218> PMID: 32932121
55. Abou-Seri S.M., Eldehna W.M., Ali M.M., Abou El Ella D.A., 1-Piperazinylphthalazines as potential VEGFR-2 inhibitors and anticancer agents: synthesis and in vitro biological evaluation, *European journal of medicinal chemistry* 107 (2016) 165–179. <https://doi.org/10.1016/j.ejmech.2015.10.053> PMID: 26590508
56. Alsaif N.A., Taghour M.S., Alanazi M.M., Obaidullah A.J., Al-Mehizia A.A., Alanazi M.M., et al, Discovery of new VEGFR-2 inhibitors based on bis ([1, 2,4 ] triazolo)[4, 3-a: 3', 4'-c] quinoxaline derivatives as anticancer agents and apoptosis inducers, *Journal of enzyme inhibition and medicinal chemistry* 36(1) (2021) 1093–1114. <https://doi.org/10.1080/14756366.2021.1915303> PMID: 34056992
57. Borenfreund E., Puerner J.A., Toxicity determined in vitro by morphological alterations and neutral red absorption, *Toxicology letters* 24(2–3) (1985) 119–124. [https://doi.org/10.1016/0378-4274\(85\)90046-3](https://doi.org/10.1016/0378-4274(85)90046-3) PMID: 3983963
58. Koch A., Tamez P., Pezzuto J., Soejarto D., Evaluation of plants used for antimalarial treatment by the Maasai of Kenya, *Journal of Ethnopharmacology* 101(1–3) (2005) 95–99. <https://doi.org/10.1016/j.jep.2005.03.011> PMID: 15878245
59. Arranz-Valsero I., Soriano-Romaní L., García-Posadas L., López-García A., Diebold Y., IL-6 as a corneal wound healing mediator in an in vitro scratch assay, *Experimental Eye Research* 125 (2014) 183–192. <https://doi.org/10.1016/j.exer.2014.06.012> PMID: 24971496
60. Zucchini N., de Sousa G., Bailly-Maitre B., Gugenheim J., Bars R., Lemaire G., et al, Regulation of Bcl-2 and Bcl-xL anti-apoptotic protein expression by nuclear receptor PXR in primary cultures of human and rat hepatocytes, *Biochimica et Biophysica Acta (BBA)-Molecular Cell Research* 1745(1) (2005) 48–58. <https://doi.org/10.1016/j.bbamcr.2005.02.005> PMID: 16085054
61. El-Zahabi M.A., Elbendary E.R., Bamanie F.H., Radwan M.F., Ghareib S.A., Eissa I.H., Design, synthesis, molecular modeling and anti-hyperglycemic evaluation of phthalimide-sulfonylurea hybrids as PPAR $\gamma$  and SUR agonists, *Bioorg. Chem.* 91 (2019) 103115. <https://doi.org/10.1016/j.bioorg.2019.103115> PMID: 31310882
62. Ibrahim M.K., Eissa I.H., Alesawy M.S., Metwaly A.M., Radwan M.M., ElSohly M.A., Design, synthesis, molecular modeling and anti-hyperglycemic evaluation of quinazolin-4 (3H)-one derivatives as potential PPAR $\gamma$  and SUR agonists, *Bioorganic & medicinal chemistry* 25(17) (2017) 4723–4744.
63. Ibrahim M.K., Eissa I.H., Abdallah A.E., Metwaly A.M., Radwan M., ElSohly M., Design, synthesis, molecular modeling and anti-hyperglycemic evaluation of novel quinoxaline derivatives as potential PPAR $\gamma$  and SUR agonists, *Biorg. Med. Chem.* 25(4) (2017) 1496–1513.
64. El-Gamal K.M., El-Morsy A.M., Saad A.M., Eissa I.H., Alswah M., Synthesis, docking, QSAR, ADMET and antimicrobial evaluation of new quinoline-3-carbonitrile derivatives as potential DNA-gyrase inhibitors, *Journal of Molecular Structure* 1166 (2018) 15–33.
65. Elkaeed E.B., Elkady H., Belal A., Alsouk B.A., Ibrahim T.H., Abdelmoaty M., et al, Multi-Phase In Silico Discovery of Potential SARS-CoV-2 RNA-Dependent RNA Polymerase Inhibitors among 3009 Clinical and FDA-Approved Related Drugs, *Processes* 10(3) (2022) 530.
66. Suleimen Y.M., Jose R.A., Suleimen R.N., Arenz C., Ishmuratova M.Y., Toppet S., et al, a New Flavonoid from *Artemisia commutata* with an In Silico Inhibitory Potential against the SARS-CoV-2 Main Protease, *Molecules* 27(5) (2022) 1636.
67. Suleimen Y.M., Jose R.A., Suleimen R.N., Arenz C., Ishmuratova M., Toppet S., et al, Isolation and In Silico Anti-SARS-CoV-2 Papain-Like Protease Potentialities of Two Rare 2-Phenoxychromone Derivatives from *Artemisia* spp, *Molecules* 27(4) (2022) 1216. <https://doi.org/10.3390/molecules27041216> PMID: 35209006
68. Alanazi M.M., Elkady H., Alsaif N.A., Obaidullah A.J., Alkahtani H.M., Alanazi M.M., et al, New quinoxaline-based VEGFR-2 inhibitors: design, synthesis, and antiproliferative evaluation with in silico docking, ADMET, toxicity, and DFT studies, *RSC Advances* 11(48) (2021) 30315–30328. <https://doi.org/10.1039/d1ra05925d> PMID: 35493991
69. Alsaif N.A., Dahab M.A., Alanazi M.M., Obaidullah A.J., Al-Mehizia A.A., Alanazi M.M., et al, New quinoxaline derivatives as VEGFR-2 inhibitors with anticancer and apoptotic activity: design, molecular modeling, and synthesis, *Bioorganic Chemistry* 110 (2021) 104807. <https://doi.org/10.1016/j.bioorg.2021.104807> PMID: 33721808

70. Mohammed S.O., El Ashry E.S.H., Khalid A., Amer M.R., Metwaly A.M., Eissa I.H., et al, Expression, Purification, and Comparative Inhibition of *Helicobacter pylori* Urease by Regio-Selectively Alkylated Benzimidazole 2-Thione Derivatives, *Molecules* 27(3) (2022) 865. <https://doi.org/10.3390/molecules27030865> PMID: 35164122
71. Alesawy M.S., Elkaeed E.B., Alsouk A.A., Metwaly A.M., Eissa I., In Silico Screening of Semi-Synthesized Compounds as Potential Inhibitors for SARS-CoV-2 Papain-like Protease: Pharmacophoric Features, Molecular Docking, ADMET, Toxicity and DFT Studies, *Molecules* 26(21) (2021) 6593. <https://doi.org/10.3390/molecules26216593> PMID: 34771004
72. Alanazi M.M., Elkady H., Alsaif N.A., Obaidullah A.J., Alanazi W.A., Al-Hossaini A.M., et al, Discovery of new quinoxaline-based derivatives as anticancer agents and potent VEGFR-2 inhibitors: Design, synthesis, and in silico study, *Journal of Molecular Structure* (2021) 132220.
73. Jo S., Kim T., Iyer V.G., Im W., CHARMM-GUI: A web-based graphical user interface for CHARMM, *Journal of computational chemistry* 29(11) (2008) 1859–1865. <https://doi.org/10.1002/jcc.20945> PMID: 18351591
74. Brooks B.R., Brooks C.L. III, Mackerell A.D. Jr., Nilsson L., Petrella R.J., Roux B., et al, CHARMM: The biomolecular simulation program, *Journal of computational chemistry* 30(10) (2009) 1545–1614. <https://doi.org/10.1002/jcc.21287> PMID: 19444816
75. Lee J., Cheng X., Swails J.M., Yeom M.S., Eastman P.K., Lemkul J.A., et al, Im, CHARMM-GUI Input Generator for NAMD, GROMACS, AMBER, OpenMM, and CHARMM/OpenMM Simulations Using the CHARMM36 Additive Force Field, *Journal of chemical theory and computation* 12(1) (2016) 405–413.